Published for SISSA by Springer

Received: *July 9, 2017*
Accepted: *September 1, 2017*
Published: *September 28, 2017*

Machine learning in the string landscape

Jonathan Carifio,[a] **James Halverson,**[a] **Dmitri Krioukov**[a,b,c] **and Brent D. Nelson**[a]

[a] *Department of Physics, Northeastern University,*
110 Forsyth Street, Boston, MA, 02115 U.S.A.
[b] *Department of Mathematics, Northeastern University,*
360 Huntington Ave, Boston, MA, 02115 U.S.A.
[c] *Department of Electrical and Computer Engineering, Northeastern University,*
360 Huntington Avenue, Boston, MA, 02115 U.S.A.

E-mail: j.carifio@neu.edu, jhh@neu.edu, dima@northeastern.edu, b.nelson@neu.edu

Abstract: We utilize machine learning to study the string landscape. Deep data dives and conjecture generation are proposed as useful frameworks for utilizing machine learning in the landscape, and examples of each are presented. A decision tree accurately predicts the number of weak Fano toric threefolds arising from reflexive polytopes, each of which determines a smooth F-theory compactification, and linear regression generates a previously proven conjecture for the gauge group rank in an ensemble of $\frac{4}{3} \times 2.96 \times 10^{755}$ F-theory compactifications. Logistic regression generates a new conjecture for when E_6 arises in the large ensemble of F-theory compactifications, which is then rigorously proven. This result may be relevant for the appearance of visible sectors in the ensemble. Through conjecture generation, machine learning is useful not only for numerics, but also for rigorous results.

Keywords: D-branes, F-Theory, Superstring Vacua

ArXiv ePrint: 1707.00655

https://doi.org/10.1007/JHEP09(2017)157

Contents

1 Introduction **1**

2 Machine learning for theoretical physicists **3**
2.1 Supervised learning 3
2.2 Unsupervised learning 4
2.3 Model evaluation 4

3 Data dive: the number of smooth F-theory compactifications **8**
3.1 Learning strategy 8
3.2 Model evaluation with 10-fold cross-validation 9
3.3 Machine learning $3d$ polytope triangulations 10

4 Conjecture generation: gauge group rank in F-theory ensembles **14**
4.1 F-theory review 14
4.2 A large ensemble of F-theory geometries 16
4.3 Data generation from random samples 19
4.4 Gauge group rank 20

5 Conjecture generation: E_6 sectors in F-theory ensembles **23**
5.1 Variable selection 23
5.2 Machine learning 25
5.3 Conjecture formulation 27
5.4 Conjecture refinement and proof 27

6 Conclusions **32**

1 Introduction

String theory is perhaps the most promising candidate for a unified theory of physics. As a quantum theory of gravity that naturally gives rise to general relativity at long distances and the building blocks for realistic particle and cosmological sectors, it satisfies a number of non-trivial necessary conditions for any unified theory. In fact, it is the only known theory that satisfies these necessary conditions. However, its extra dimensions of space allow for many compactifications to four dimensions, which give rise to a large landscape of vacua that may realize many different incarnations of particle physics and cosmology. Taming the landscape is therefore a central problem in theoretical physics, and is critical to making progress in understanding unification in string theory.

In this paper, we treat the landscape as what it clearly is: a big data problem. In fact, the data that arise in string theory may be the largest in science. For example, in type

IIb compactifications there are many possible Ramond-Ramond background fluxes that depend on the topology of the extra dimensions. This is the context for the oft-quoted $O(10^{500})$ type IIb flux vacua [1–3], though in recent years this number has grown to an estimated $O(10^{272,000})$ [4] . Recently [5], the number of geometries has grown beyond the early flux number to $\frac{4}{3}\times 2.96\times 10^{755}$, which is known to only be a lower bound. Dealing with these large numbers is exacerbated by the computational complexity of the landscape [6–9], making it even more clear that sophisticated techniques are required.

How should one treat ensembles so large that they forbid explicit construction? One analytic technique is algorithmic universality. Rather than deriving universality from exploration of a constructed ensemble, algorithmic universality is derived instead from a concrete construction algorithm. This idea, while obvious, was exemplified in [5] and used to demonstrate universal features in the ensemble of 10^{755} F-theory geometries. For example, knowledge of the construction algorithm demonstrated that the probability P_{NHC} of having clusters of non-trivial seven-branes is $1 > P_{\text{NHC}} \geq 1 - 1.07 \times 10^{-755}$, and also that the probability P_G of having a particular minimal geometric gauge group G with $\text{rk}(G) \geq 160$ is $1 > P_G \geq .999995$. This degree of control over such a large ensemble is ideal, but in many physically interesting cases such precise construction algorithms are not yet known. In this case, one must either develop such construction algorithms, which may not always be possible, or utilize other techniques.

The other possibility is to use numerical techniques from data science, and in some cases we will see that these numerical techniques can lead to rigorous results. Specifically, we will employ modern machine learning techniques to study the landscape. Machine learning is a broad term for a wide variety of techniques that allow a computer to develop prediction models for complex datasets or to extract features. It has led to veritable revolutions in a number of fields, from genotyping and gene expression to oceanography and climate science. We will provide a review of basic machine learning techniques in section 2.

It is easy to imagine a number of broad ways in which machine learning could be of use in string theory, as well as mathematics and theoretical physics more broadly.

- *Deep Data Dives.* Via training a model on a subset of an ensemble, it is sometimes feasible to make high accuracy feature predictions that are much faster than conventional techniques, allowing for far greater exploration of the dataset.

- *Conjecture Generation.* The decision function of a trained model may naturally lead to a sharp conjecture that can be rigorously proven.

- *Feature Extraction.* When input data is of high dimensionality, or exhibits redundant information, models can identify those properties (*features*) of the data that are most correlated with desired outcomes. This is often one of the primary goals of landscape surveys in string theory.

Many other possibilities may arise as new machine learning techniques are developed by computer scientists.

In this paper we will present one example of a data dive, and two of conjecture generation. The data dive and one of the generated conjectures are known results, while the other generated conjecture is a genuinely new result that would have been more difficult to obtain without machine learning.

Summary of results. The layout of our paper and the summary of our results are as follows.

The data dive is used to study the geometries relevant for certain four dimensional F-theory compactifications. Specifically, in section 3 we use machine learning to compute the number of fine regular star triangulations (FRST) of three-dimensional reflexive polytopes, each of which determines a smooth F-theory compactification to four-dimensions, amongst other possible applications. These results compare well to known results about the number of FRST of those polytopes. In the future, similar techniques will be used in the case of four-dimensional reflexive polytopes, which will provide an upper-bound estimate of the number of Calabi-Yau threefolds in the Kreuzer-Skarke set.

The conjecture generation arises in the context of the ensemble of $\frac{4}{3} \times 2.96 \times 10^{755}$ F-theory geometries. We utilize random sampling to generate data that will be used to train models. In section 4 we train models that accurately predict the rank of the gauge group in each geometry. Study of the decision function and properties of the data structure give rise to a sharp conjecture that may be rigorously proven; in fact, the result was known, though the conjecture was not previously arrived at via machine learning. The general process by which that conjecture was generated is applicable in other contexts. In section 5 we use this process to generate a conjecture regarding conditions under which E_6 arises in the ensemble. The conjecture is proven, which leads to a computation of the probability of E_6 in the ensemble. Comparing to five independent sets of $2,000,000$ random samples, the predictions match quite well.

We find it promising that new rigorous results may arise from conjectures that would be difficult to arrive at without the help of machine learning. Further areas of promise for utilizing machine learning in string theory will be suggested in the concluding section.

While we were completing this work, [10] and [11] appeared. Those works also utilize learning to study the landscape, but they differ in specific techniques and physical applications. [12] used machine learning to find the minimum volumes of Sasaki-Einstein manifolds.

2 Machine learning for theoretical physicists

Since machine learning is not part of the everyday lexicon of a theoretical physicist, in this section we would like to review the basics of the subject, including all of the techniques that we utilized in this paper. The subject has a rich literature; for a more in-depth introduction we recommend the textbooks [13, 14]. Here, we focus on explaining the basic ideas behind supervised learning, unsupervised learning, and model evaluation.

2.1 Supervised learning

Machine learning is a set of algorithms that trains on a data set in order to make predictions on unseen data. As such, simple least-squares regression — a tool with which every scientist is familiar — is seen as the most humble form of machine learning. Modern techniques can be incredibly sophisticated, but it is worth remembering that the output from most machine learning algorithms is a function (commonly called a *model*): it takes a specified set of inputs and produces a unique output value for the characteristic in question.

The procedure described above is commonly referred to as *supervised* machine learning, or simply *supervised learning*. For supervised learning, the training step is performed by allowing the algorithm to experience a number of input → output pairs. This is the most common (and generally most successful) form of machine learning. All of the results in this paper, as well as those that have appeared recently in the literature [10–12], arise from the application of supervised machine learning.

For physics applications, the input data may be mathematical and abstract. Examples may include the vertices of a polytope in $\mathbb{Z}^3$ or $\mathbb{Z}^4$ or the tensor of intersection numbers of divisors and curves on a Calabi-Yau threefold. The outputs are generally meaningful physical quantities, such as the presence of an orientifold involution or the rank of a gauge group.

In order to effectively utilize supervised machine learning, the physicist must have identified these physically relevant output variables so as to prepare a relevant training sample in the first place. When no such outputs are identified, we refer to the procedure as *unsupervised machine learning*.

2.2 Unsupervised learning

As no particular output is specified in unsupervised learning, the goal of an algorithm is often more modest. For example, one might employ a *clustering algorithm* that seeks to group inputs according to which cases are most 'similar' in some fashion. Another common goal of unsupervised learning is *dimensionality reduction*, in which a large dataset of high dimensionality is transformed into a smaller dataset through a form of coarse-graining, with a goal of retaining the essential global properties of the data. Both clustering and dimensionality reduction are employed in supervised learning as well, where the latter is often referred to as *factor analysis*, or *principal component analysis*.

The datasets which concern us in string theory are often cases in which the data is itself constructed through well-defined mathematical algorithms, with a specific physics goal in mind. As such, there is less need for unsupervised learning in as much as the outcome of unsupervised machine learning is often merely a step in the direction of more effective supervised learning. Again, the lack of a specific goal, or output variable, in unsupervised learning makes it difficult to answer the question of how well the algorithm has performed. This is called *model evaluation*.

2.3 Model evaluation

In supervised learning, model evaluation is more straight-forward. An obvious manner in which to proceed is as follows. Let us take the total set of cases in which input → output pairs are known, and divide it into a *training set* and a *test set*. This is called a *train-test split*. The model is then developed through training on the training set. Once created, the model is then evaluated on the test set. The performance of the model can then be evaluated through normal statistical means.

When computational cost is not at issue, a *k-fold cross-validation* procedure is a better training method. In this case, the data is divided into k equal subsets. Our model will now be trained k separate times, in each reserving only one of the k partitions (or 'folds') for testing, and using the other $k-1$ folds for training. This method has several advantages. First, it minimizes training-sample bias, in which our training data happens to be different qualitatively from our testing data. Second, while a simple train-test split might train on just 50% of the data, a ten-fold cross-validation (which we use in this paper) will train on 90% of the available data. Finally, we will evaluate the efficacy of our model multiple times on different independent pieces of our data, thereby giving us a measure of how robust our model is to perturbations on the data.

The correct model evaluation metric depends on the type of algorithm being employed. If the goal is one of clustering, such as the *binary classification* problem, we are usually concerned with the *accuracy* of the model. Thus, if the goal is to predict, given the input data, whether or not a certain number is non-vanishing, then the model will return a function which varies from zero to one. The accuracy can then be computed from the fraction of "true" cases in the test data for which the model returns unity. A more generalized evaluation tool is the *confusion matrix*, which also returns the number of "false-positives" and "false-negatives".

In physics applications, we are more often trying to predict a continuous real number, which is a form of *regression analysis.* The evaluation of regression algorithms is typically a statistical goodness-of-fit variable. We will discuss a number of such algorithms below.

Techniques used in this paper. There are a number of supervised learning algorithms that we use in this paper: Linear Regression, Logistic Regression, Linear Discriminant Analysis, k-Nearest Neighbors, Classification and Regression Tree, Naive Bayes, and Support Vector Machine. In the following we will briefly describe the workings of each algorithm, as well as the pros and cons of each, in cases that they are known.

Linear Regression (LIR) is the analog of least-squares regression for the case of multiple input variables. If the output quantity is denoted by y, then the model seeks a set of w_i and an intercept b such that $y = b + \sum_i^n w_i x_i$, where n is the number of input properties, labeled by x_i. This method can be generalized to allow for constraints on the allowed weights — perhaps to reflect known physical requirements.

Logistic Regression (LR) gets its name from its reliance on the *logistic function*, sometimes also referred to as the *sigmoid function.* As this function interpolates between zero and unity, it is often used by statisticians to represent a probability function. As such, logistic regression (despite its name) is most often used in binary classification problems. While a linear method, logistic regression is more general than linear regression in that predictions are no longer merely linear combinations of inputs. The advantages of this technique include its relative ease of training and its suitability for performing factor analysis. In addition, logistic regression is more resistant to the peril of *overfitting* the input data, in which noise (random fluctuations) in the input data is incorporated into the model itself, thereby limiting its ability to correctly predict on newly encountered data.

k-Nearest Neighbors (KNN) is an algorithm that develops a prediction for a particular output by looking at the outputs for the k closest 'neighbors' in the input space. Once a metric on the input parameter space is specified, the k-closest neighbors are identified. The predicted output may then be as simple as the weighted average of the values of the neighbors. This method has the advantage of extreme conceptual simplicity, though it can be computationally costly in practice. The method is thus best suited to input data with low dimensionality — or where factor analysis reveals a low effective dimensionality. The method will be less useful in cases where the data is of high dimensionality, where some data spans a large range of absolute scales, or where the data cannot be readily expressed in the form of a simple n-tuple of numbers.

Classification and Regression Tree (CART) is the name given to *decision tree* approaches to either classification or regression problems. These algorithms divide up the input feature space into rectangular regions, then coarse grain the data in these regions so as to produce "if-then-else" decision rules. In so doing, such methods generally identify feature importance as an immediate by-product of the approach. Decision trees are not linear in the parameters: they are able to handle a mix of continuous and discrete features and the algorithms are invariant to scaling of the data. By their very nature, however, they are ill-suited to extrapolation to features beyond those of the training data itself.

Naive Bayes (NB), as the name suggests, seeks to compute the probability of a hypothesis given some prior knowledge of the data. More specifically, we are interested in the most important features of the data, and we assume that these features are conditionally independent of one another (hence 'Naive' Bayes). A great number of hypothesis functions are created from the data features, and the one with the maximum *a posteriori* probability is selected. This linear method is generally used in classification problems, but can be extended to continuous prediction in *Gaussian Naive Bayes*. Here, each feature is assigned a distribution in the data; for example, a Gaussian distribution, which can be classified simply by the mean and the variance of that feature across the dataset. This makes Gaussian NB very efficient to implement on data sets in which the input data is effectively continuous in nature, or of high dimensionality. However, if input data is known to be highly correlated, we should expect NB algorithms to perform poorly relative to other methods.

Linear Discriminant Analysis (LDA) has similarities to both logistic regression and Gaussian naive Bayes approaches. It assumes that the data has a Gaussian distribution in each feature, and that the variance for each feature is roughly equivalent. Like NB methods, it then builds and evaluates a probability function for class membership, and is thus generally used in classification problems. Despite the name, LDA approaches can be effectively non-linear, by constructing a *feature map* that transforms the raw input data into a higher-dimensional space associated with *feature vectors* (sometimes called the *kernel trick*). In this, LDA algorithms share many methods with principal component analysis (PCA). The latter is often described as 'unsupervised' in the sense that its goal is to find directions in feature space that maximize variance in the dataset, while ignoring class labels, while LDA is 'supervised' in the sense that it seeks to find directions in feature space that maximize the distance between the classes.

Support Vector Machine (SVM) is another technique that involves feature space, and is often one of the more powerful supervised learning algorithms. The feature space is partitioned using linear separation hyperplanes in the space of input variables. The smallest perpendicular distance from this hyperplane to a training data point is called the *margin*. The optimal dividing hyperplane is thus the one with the maximal margin. The training data that lie upon these margins are known as the *support vectors* — once these points are identified, the remainder of the training data becomes irrelevant, thereby reducing the memory cost of the procedure. At this point we have a support vector classifier (SVC). The method can be generalized by using the kernel method described above, which is necessary in cases for which the desired outputs overlap in feature space. In such cases the generalization is referred to as the support vector machine algorithm. SVM can be adapted to perform regression tasks as well (support vector regression).

Techniques not used in this paper. In the course of preparing this work, other examples of using machine learning techniques in string theory have appeared. The techniques in these cases generally involve the use of *neural networks*, whose properties we briefly describe in this subsection.

The basic building block of a neural network is the *perceptron*, which can be described as a single binary classification algorithm. These algorithms are generally linear, and thus each of the techniques described above, and used in this paper, can be thought of as individual perceptrons. Multi-layer perceptron (MLP) models are generalization of the linear models described above in that multiple techniques are layered between the input data and the output predictions. It is these collections of perceptrons that tend to be called neural networks. The simplest cases are feed-forward neural networks, in that each layer delivers its output as the input to the subsequent layer. More sophisticated approaches allow flow of information in both directions, thereby producing feedback. These latter cases more closely approximate the structure of true biological neural networks.

Like the cases described above, neural networks themselves can be supervised or unsupervised. That is, neural networks can be trained on data in which input → output pairs are known, or allowed to perform clustering or dimensionality reduction tasks on data where no outputs are specified. Furthermore, the individual layers in the MLP can be chosen by the model-developer in advance, or allowed to evolve through feedback, with the latter case introducing an element of unsupervised learning into the MLP.[1]

[1] It is common to use the phrase "deep learning" to indicate any machine learning technique that involves a neural network model, though often this phrase is restricted to those cases which involve some element of unsupervised learning.

Neural networks and single-model methods generally fare comparably, though each has its place and relative advantages. By adding layers and feedback channels, a neural network can be designed with a large number of free, tunable parameters. This can lead to the problem of overfitting, however. On the other hand, such frameworks are generally suited to many forms of input data, or highly heterogeneous input data. A key disadvantage is the fact that the output of a neural network training tends to be a 'black box', which makes such techniques less useful for feature extraction or conjecture generation, though still quite powerful for deep data dives.[2] For these various reasons we have chosen to work with the single-algorithm approach, and will generally use the simplest such approaches to achieve the goals of this paper.

3 Data dive: the number of smooth F-theory compactifications

In this section we use machine learning to estimate the number of fine regular star triangulations (FRST) of three-dimensional reflexive polytopes [15]. Each such FRST determines a smooth weak-Fano toric variety. These varieties and their number are interesting for at least three reasons: their anti-canonical hypersurfaces give rise to K3 surfaces that can be used for six-dimensional string compactifications, they give rise to smooth F-theory compactifications without non-Higgsable clusters [16], and they serve as a starting point for topological transitions from which the ensemble of 10^{755} F-theory geometries arises.

3.1 Learning strategy

Let Δ° be a $3d$ reflexive polytope. Such an object is the convex hull of a set of points $\{v\} \subset \mathbb{Z}^3$ that satisfies the reflexivity condition, i.e. that the dual polytope

$$\Delta := \{m \in \mathbb{Z}^3 \mid m \cdot v \geq -1 \; \forall v \in \Delta^\circ\} \tag{3.1}$$

is itself a lattice polytope. There are 4319 such polytopes, classified by Kreuzer and Skarke [15]. A triangulation of Δ° is said to be fine, regular, and star if all integral points of Δ° are used, the simplicial cones are projections of cones from an embedding space, and all simplices have the origin as a vertex. We refer to these as FRSTs.

A weak-Fano toric variety may be associated to each such FRST of a $3d$ reflexive polytope, where $h^{11}(B) = |\{v\}| - 3$ is the dimension of the Dolbeault cohomology group $H^{11}(B)$.[3] This integer measures the number of independent cohomologically non-trivial $(1,1)$-forms on B, or alternatively (via duality) the number of divisor classes. Such topological quantities are central to many aspects of the physics of an F-theory compactification on B.

The number of FRSTs of these polytopes was computed for low $h^{11}(B)$ in [16], where B is the toric variety associated to the FRST, and estimates were provided for the remainder based on techniques in the triangulation literature. Here we instead wish to estimate the number of FRSTs of the $3d$ reflexive polytopes using machine learning.

[2] These same criticisms could be leveled against the most sophisticated SVM techniques, which are often comparable to neural networks in complexity.

[3] We remind the reader that we employ the notation $|\{X\}|$ to indicate the cardinality of the set X.

Our method is to estimate the number of FRSTs of the $3d$ reflexive polytopes as the product of the number of fine regulation triangulations (FRTs) of its codimension one faces, which are known as facets. This was demonstrated to be a good approximation in [16], and the number of FRTs of the facets was explicitly computed for $h^{11}(B) \leq 22$, where all B arising from FRSTs of $3d$ reflexive polytopes have $h^{11}(B) \leq 35$. In this work, we will utilize machine learning to train a model to predict the number of FRTs per facet, and then we will use the trained algorithm to estimate the number of FRSTs of the $3d$ reflexive polytopes. We will see that the results are in good agreement with those of [16], though derived in a different manner.

The vertices of Δ° determine Δ°, and therefore its FRSTs may be computed from this data. However, for higher $h^{11}(B)$ the number of integral points in Δ° also increases, which increases the number of FRSTs and therefore also the likelihood that the computation does not finish in a reasonable amount of time. As this occurs, the number of FRTs of each facet also typically increases. The number of FRTs of a facet F increases with its number of points n_p, interior points n_i, boundary points n_b, and vertices n_v, which are of course related. To each facet, which is a $2d$ polyhedron, we therefore associate a 4-tuple (n_p, n_i, n_b, n_v). Using machine learning we will train a model A to predict the number of FRTs of each facet given the 4-tuple. This gives a chain of operations

$$F \longrightarrow (n_p, n_i, n_b, n_v) \xrightarrow{A} n_T, \tag{3.2}$$

that predicts the n_T, the number of FRTs of F. It is obvious that n_T will depend on the 4-tuple, but the question is to what extent.

We have attempted to choose the training variables wisely based on knowledge of the dataset. This is supervised learning.

3.2 Model evaluation with 10-fold cross-validation

We begin by utilizing 10-fold cross-validation to determine which machine learning algorithm gives rise to the model with the best predictions for n_T. There are two critical considerations that will enter into our analysis. First, in order to extrapolate to very high h^{11} with reasonable confidence, we would like to train our models for $h^{11} < 19$ so that we can test the trained model on known results for the number of facet FRTs for polytopes with $h^{11} = 19, 20, 21$. We therefore train on data with $h^{11} \leq h^{11}_{\text{max}} < 19$. Second, since there are very few triangulations for low h^{11} and this may negatively affect the model, we will train on data with $h^{11} \geq h^{11}_{\text{min}}$. We take $h^{11}_{\text{min}} \in \{1, 6, 10\}$ and $h^{11}_{\text{max}} \in \{14, 16, 18\}$, and therefore we perform a 10-fold cross validation on nine different ranges $h^{11}_{\text{min}} \leq h^{11} \leq h^{11}_{\text{max}}$.

For each, we test four different algorithms:

- LDA: Linear Discriminant Analysis
- KNNR: k-Nearest Neighbors Regression
- CART: Classification and Regression Trees
- NB: Naive Bayes,

which are described in section 2. The scoring metric that we use is the mean absolute percent error, which is defined to be

$$\text{MAPE} := \frac{100}{n} \times \sum_{i=1}^{n} \left| \frac{A_i - P_i}{A_i} \right| , \tag{3.3}$$

where n is the number of values, and P_i and A_i are the predicted and actual values for the output; here n_T of the i^{th} facet. In k-fold validation, the scoring is done k times (using each fold as the validation set once). We then average the MAPE values from each test to obtain the final scoring metric. Finally, for each algorithm trained on the data with $h^{11}_{\text{min}} \leq h^{11} \leq h^{11}_{\text{max}}$, we predict n_T for each polytope with $h^{11} = 19, 20, 21$ and present the average MAPE.

The results of this analysis are presented in table 1. The minimal MAPE for the training set occurs for KNNR with $(h^{11}_{\text{min}}, h^{11}_{\text{max}}) = (1, 14)$; however, we see that this case has higher MAPE for n_T of facets at higher h^{11}. The lowest MAPE at $h^{11} = 21$ occurs in CART examples with $(h^{11}_{\text{min}}, h^{11}_{\text{max}}) = (6, 18)$ and $(h^{11}_{\text{min}}, h^{11}_{\text{max}}) = (10, 18)$, with slightly better performance in the former case. In table 2 we present the results of a similar analysis that fixes h^{11}_{max} and CART while scanning over h^{11}_{min}. The results are similar in all cases, though the MAPE is slightly lower in the case $h^{11}_{\text{min}} = 4$, which seems to be a point at which the anomalous polytopes at very low h^{11} are safely discarded.

As a result of this analysis, we choose to model the FRTs of facets F of $3d$ reflexive polytopes via a classification and regression tree (CART) with $h^{11}_{\text{min}} = 4$. We will train the model on $h^{11}_{\text{min}} = 4 \leq h^{11} \leq 21$ since the exact number of FRTs at $19 \leq h^{11} \leq 21$ should increase accuracy in the extrapolation to $h^{11} > 21$.

Training with these parameters using 10-fold cross validation, we find that the MAPE is $6.38 \pm 1.04\%$; this is on par with the results of table 1. For a broader view of the model predictions, see figure 1. Both of the plots are a measure of the relative factors

$$R_i := \frac{P_i}{A_i} \tag{3.4}$$

that determine the factor by which the predicted value P_i for n_T of a facet is off from the actual value A_i. We have computed A_i for all facets in all polytopes up through $h^{11} = 21$. The plot on the left is a box plot of the values of n_T that occur at each respective value of h^{11}. Though a few outlier predictions are off from the actual values by a factor of 5 to 7, note that the orange band denotes the median which is 1.0, and the would-be boxes of the box plot are absent since their boundaries would denote the first and third quartile, both of which are also 1.0. The plot on the right computes the percent with $\frac{1}{2} < R_i < 2$; over 96% of the n_T of facets, for all h^{11}, are within a factor of 2 of their actual value.

3.3 Machine learning $3d$ polytope triangulations

Given the accuracy of this model, we would now like to compute the average number of FRSTs per polytope as a function of $h^{11}(B)$. This was done in [16], and it will be instructive to see whether machine learning recovers those results, and also where it has difficulties.

				Extrap. $h^{11} = 19$		Extrap. $h^{11} = 20$		Extrap. $h^{11} = 21$	
Alg.	h^{11}_{min}	h^{11}_{max}	Train MAPE	MAPE	STDEV	MAPE	STDEV	MAPE	STDEV
LDA	1	14	14.3	28.5	70.0	37.4	85.2	38.0	81.4
KNNR	1	14	4.1	17.4	45.0	19.5	47.2	24.7	53.7
CART	1	14	5.6	18.0	45.3	17.0	39.0	24.3	56.4
NB	1	14	11.2	26.4	58.3	31.9	68.1	35.3	71.7
LDA	1	16	14.5	23.1	68.7	31.9	87.3	30.8	80.4
KNNR	1	16	4.4	15.0	43.9	20.0	63.6	26.6	76.1
CART	1	16	5.6	14.2	42.4	14.5	43.3	20.9	58.5
NB	1	16	10.9	21.3	56.6	28.2	70.7	29.8	70.3
LDA	1	18	15.1	20.9	67.9	28.8	86.8	28.7	79.9
KNNR	1	18	4.7	12.2	33.0	12.0	46.7	19.9	61.0
CART	1	18	6.2	11.7	41.0	11.1	40.5	18.5	53.9
NB	1	18	11.9	19.3	55.6	25.2	69.9	27.4	69.6
LDA	6	14	14.6	26.8	70.0	35.1	85.4	35.7	81.7
KNNR	6	14	4.4	18.4	39.4	21.9	50.1	27.0	59.5
CART	6	14	5.3	18.2	45.6	17.5	40.5	25.0	58.0
NB	6	14	10.7	25.3	58.1	31.6	67.8	34.1	71.5
LDA	6	16	14.8	22.4	68.6	31.1	87.3	30.0	80.3
KNNR	6	16	4.7	13.8	40.7	16.8	55.2	22.9	64.8
CART	6	16	6.0	13.3	41.6	13.4	41.9	19.4	53.3
NB	6	16	11.1	19.9	56.4	27.9	70.7	29.0	70.3
LDA	6	18	14.0	20.4	67.9	28.2	86.7	28.2	80.3
KNNR	6	18	5.1	10.8	38.9	11.1	48.4	18.3	60.0
CART	6	18	6.1	11.8	40.8	10.5	40.0	17.5	54.4
NB	6	18	12.6	18.3	55.6	24.6	69.8	26.0	70.2
LDA	10	14	12.7	16.7	44.1	17.5	47.5	22.8	56.9
KNNR	10	14	5.4	16.9	44.7	19.7	49.1	25.4	58.8
CART	10	14	6.2	16.3	43.9	16.3	44.5	21.6	54.4
NB	10	14	10.3	22.7	58.2	30.7	71.6	32.0	71.9
LDA	10	16	12.9	14.8	42.9	15.6	46.0	21.7	56.4
KNNR	10	16	5.4	14.4	35.5	17.1	59.9	25.1	77.7
CART	10	16	6.3	14.0	42.1	14.2	44.8	21.0	55.2
NB	10	16	10.5	19.8	56.5	28.3	70.7	29.1	70.5
LDA	10	18	12.9	12.6	41.0	12.1	43.5	18.6	54.7
KNNR	10	18	5.9	11.5	38.7	12.4	46.9	19.5	59.2
CART	10	18	7.2	12.4	41.0	11.1	40.4	17.9	53.6
NB	10	18	11.2	17.9	55.5	25.2	69.8	25.9	69.6

Table 1. Model discrimination and higher h^{11} testing for the number of FRTs of $3d$ reflexive polytopes. Train MAPE is the mean average percent error of the algorithm of a given type, averaged across the ten training runs, trained on the exact number of FRTs for $h^{11}_{\text{min}} \leq h^{11} \leq h^{11}_{\text{max}}$. The STDEV is the standard deviation of the ten training runs about the MAPE value. Both MAPE and STDEV are presented for model predictions for $h^{11} = 19, 20, 21 > h^{11}_{\text{max}}$.

				Extrap. $h^{11} = 19$		Extrap. $h^{11} = 20$		Extrap. $h^{11} = 21$	
Alg.	h^{11}_{min}	h^{11}_{max}	Train MAPE	MAPE	STDEV	MAPE	STDEV	MAPE	STDEV
CART	1	18	6.2	11.9	41.2	11.1	40.5	18.5	53.9
CART	2	18	5.6	11.8	40.5	10.4	39.3	17.7	53.7
CART	3	18	5.7	11.5	40.4	10.3	39.3	17.7	54.5
CART	4	18	5.5	11.2	40.1	10.5	40.0	17.4	54.4
CART	5	18	6.0	12.1	41.0	12.2	41.4	19.3	55.2
CART	6	18	6.2	11.6	40.6	10.5	40.0	17.5	54.4
CART	7	18	5.9	11.5	40.5	10.5	40.0	17.5	54.4
CART	8	18	6.5	11.6	40.5	10.5	40.0	17.6	54.4
CART	9	18	6.8	12.5	41.1	11.6	40.8	18.9	54.2
CART	10	18	7.2	12.1	40.7	11.1	40.4	17.9	53.6

Table 2. Refinement of CART algorithms for final model selection.

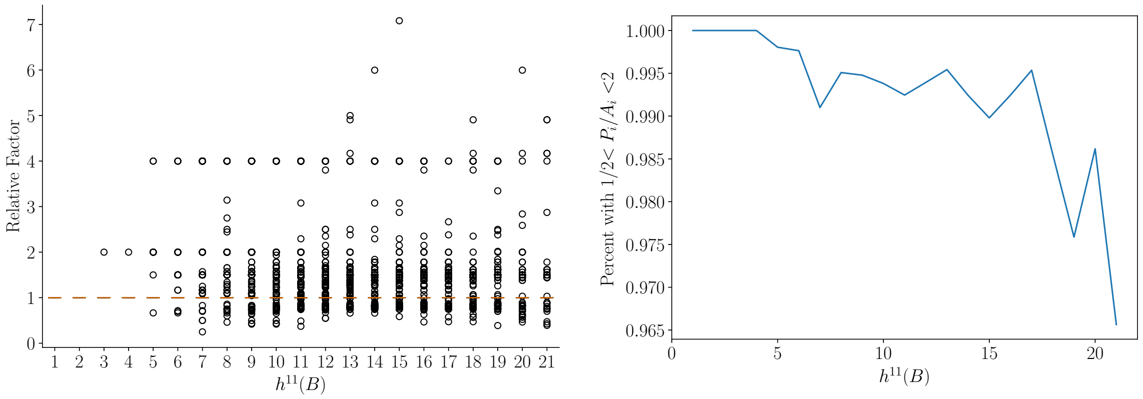

Figure 1. Left: box plot for the relative factor R_i, which is the predicted number of FRTs of each facet over the actual number. The median, first, and third quartiles are precisely at the desired value 1, though outliers do exist. Right: the percent of facets for which the predicted number of FRTs is within a factor of two of the action value.

Specifically, letting $n_T(F)$ be the number of FRTs of F computed by our model, we use the approximation discussed in [16]

$$n_{\text{FRST}}(\Delta^\circ) \simeq \prod_{F \in \Delta^\circ} n_T(F). \tag{3.5}$$

Summing over all polytopes at a given h^{11} and averaging, we define

$$\overline{n_{\text{FRST}}}(h^{11}) := \frac{\sum_{\Delta^\circ \text{ at } h^{11}} \;\; n_{\text{FRST}}(\Delta^\circ)}{\sum_{\Delta^\circ \text{ at } h^{11}} \;\; 1}. \tag{3.6}$$

This average number of triangulations per polytope at a fixed value of h^{11} is presented in figure 2. The red line, gray stars, and blue dots were obtained in [16], where the gray stars and blue dots were predicted with different methods. The green dots are the new

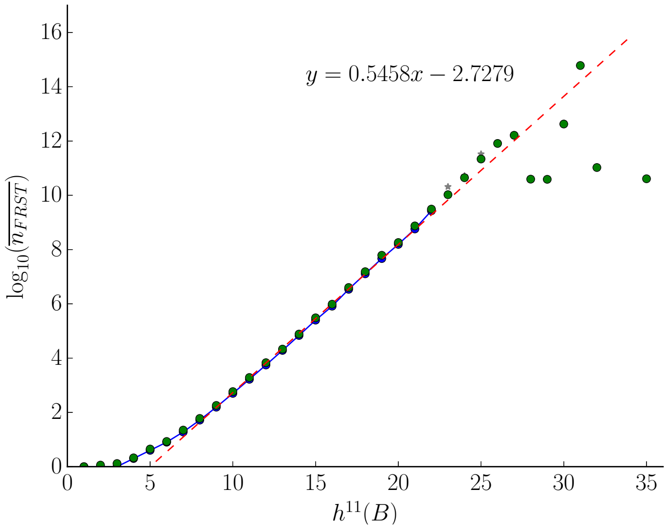

Figure 2. The logarithm of the average number of FRST per polytope. The green dots are predictions of our learned model, and the rest of the data is from [16]. Note the accuracy of model in recovering known results represented by the blue dots and grey stars. The erratic behavior for $h^{11} \geq 27$ correlates with being the tail of the polytope distribution.

predictions of our model. The predictions are so accurate that the green dots are mostly covering the blue dots, when they exist.

It is also important that our model makes accurate predictions beyond the data on which it trained. Specifically, it trained on data with $h^{11} \leq 21$ and the predicted values at $h^{11} = 22, 23, 24, 25$ are in good agreement with the results of [16]. The model also makes good predictions at $h^{11} = 26, 27$ when comparing to the extrapolation of the best fit line. We see that our model made six accurate predictions for $\overline{n_{\text{FRST}}}(h^{11})$ for h^{11} values that it was not trained upon. This demonstrates the power of machine learning to find hidden dependencies in the data that allow for extrapolation beyond the training set.

Note, however, that the machine learning model predicts erratic behavior for $h^{11} > 27$. While a priori this may be considered a prediction, the data points are inconsistent with bounds derived in [16] utilizing results in the triangulation literature. Figure 3 demonstrates that around this h^{11} value the number of facets and polytopes at a fixed value of h^{11} has dropped significantly relative to lower h^{11}. This, together with the violation of the analytic bound, leads to the conclusion that the erratic behavior for $h^{11} > 27$ may be due to being in the tail of the distribution; see values of $h^{11} > 27$ in figure 3.

However, the machine learning model predictions for the bulk of the polytope distribution picks out the correct line for $\log_{10}(\overline{n_{\text{FRST}}})$. This line, when extrapolated to the highest polytope h^{11}, which is $h^{11} = 35$, is in agreement with the bound

$$5.780 \times 10^{14} \lesssim n_{\text{FRST}} \lesssim 1.831 \times 10^{17}, \tag{3.7}$$

which was obtained in [16].

In conclusion, our model that used a 10-fold cross-validated and parameter optimized classification and regression tree accurately predicts the average number of FRSTs in the

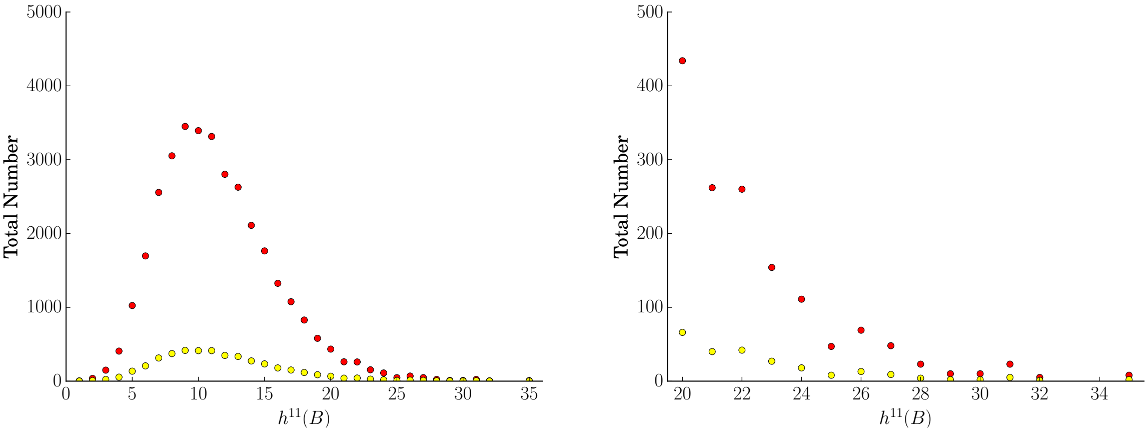

Figure 3. Red (blue) dots are the total number of facets (reflexive polytopes) at a given value of $h^{11}(B)$. Left: the full plot. Right: magnification of the $h^{11} \geq 20$ region.

bulk of the distribution for the number of polytopes and facets as a function of h^{11}. It would be interesting in the future to determine methods that minimize the error in the tail of the distribution, but we emphasize that the extrapolated best fit line of the machine learning model prediction does give $n_{\text{FRST}} \sim O(10^{15})$–$O(10^{16})$ at $h^{11} = 35$ as expected from the analytic results of [16].

4 Conjecture generation: gauge group rank in F-theory ensembles

In this section, and section 5, we will generate conjectures related to the physics of an ensemble of $\frac{4}{3} \times 2.96 \times 10^{755}$ F-theory compactifications that recently appeared in the literature [5]. This ensemble exhibited algorithmic universality, which is universality derived from a precise construction algorithm rather than a constructed ensemble. Universal features included non-Higgsable clusters with extremely large and calculable gauge groups.

4.1 F-theory review

F-theory [17, 18] is a non-perturbative formulation of the type IIb superstring in which the axiodilaton $\tau = C_0 + ie^{-\phi}$ varies holomorphically over extra dimensions of space B. This variation is conveniently encoded in the geometry of a Calabi-Yau elliptic fibration, in which τ is the complex structure of the elliptic curve that varies over the base B. By a theorem of Nakayama [19], every elliptic fibration is birationally equivalent to a Weierstrass model

$$y^2 = x^3 + fx + g, \tag{4.1}$$

where x, y are coordinates on the elliptic curve and $f \in \Gamma(\mathcal{O}(-4K))$ and $g \in \Gamma(\mathcal{O}(-6K))$ are global sections of the states line bundles, with $-K$ the anticanonical class on B. Practically, this simply means that f and g are homogeneous polynomials in appropriate coordinates on B. Seven-branes are localized on the discriminant locus

$$\Delta = 4f^3 + 27g^2 = 0, \tag{4.2}$$

F_i	l_i	m_i	n_i	Sing.	G_i
I_0	≥ 0	≥ 0	0	none	none
I_n	0	0	$n \geq 2$	A_{n-1}	SU(n) or Sp$(\lfloor n/2 \rfloor)$
II	≥ 1	1	2	none	none
III	1	≥ 2	3	A_1	SU(2)
IV	≥ 2	2	4	A_2	SU(3) or SU(2)
I_0^*	≥ 2	≥ 3	6	D_4	SO(8) or SO(7) or G_2
I_n^*	2	3	$n \geq 7$	D_{n-2}	SO$(2n-4)$ or SO$(2n-5)$
IV^*	≥ 3	4	8	E_6	E_6 or F_4
III^*	3	≥ 5	9	E_7	E_7
II^*	≥ 4	5	10	E_8	E_8

Table 3. Kodaira fiber F_i, singularity, and gauge group G_i on the seven-brane at $x_i = 0$.

where the elliptic fiber becomes singular. If $x_i = 0$ is a component of the discriminant locus, then the multiplicity of vanishing $\text{mult}_{x_i}(f, g, \Delta) = (l_i, m_i, n_i)$ of f, g and Δ along $x_i = 0$ determines (up to monodromy, see e.g. [20]) the gauge group on $x_i = 0$ according to the Kodaira classification, which is presented in table 3. These groups can be understood via smoothings of the geometry and associated Higgs mechanisms; for smoothings via Kähler resolution and complex structure deformation see e.g. [21–25] and [26–29], respectively.

Typically, the topological structure of the extra spatial dimensions B forces the existence of non-trivial seven-branes on fixed divisors. Such seven-branes are referred to as non-Higgsable seven-branes (NH7), as their inability to move obstructs the Higgs mechanism that would arise from brane splitting. NH7 usually come in sets, and they may intersect, forming a non-Higgsable cluster [30] (NHC). Mathematically the origin of this mechanism is simple: if the polynomials f and g are chosen to have all possible monomial coefficients non-zero and generic, then there may be components (factors)

$$f = F \prod_i x_i^{l_i} \qquad g = G \prod x_i^{m_i}, \tag{4.3}$$

where F and G may themselves be non-trivial polynomials. If $l_i, m_i > 0$, then there is a seven-brane on $x_i = 0$ of a type that can be determined from table 3 and the fact that $n_i = \min(3l_i, 2m_i)$. Non-Higgsable clusters are easily exemplified; for example, in a $6d$ F-theory compactification on the Hirzebruch surface $\mathbb{F}_3$, there is a non-Higgsable SU(3) on the -3 curve. That theory is non-Higgsable because the SU(3) theory has no matter.

There are a number of interesting recent results about non-Higgsable clusters and their importance in the $4d$ F-theory landscape. They exist for generic vacuum expectation values of the complex structure moduli, and therefore obtaining gauge symmetry does not require moduli stabilization to fix vacua on subloci in moduli space [31], which can occur at high codimension [32, 33], though the problem is not as severe [16] as initially thought. Strong coupling is generic [34], and some of the structures of the standard model may arise naturally [31]. They also arise in the particular geometry $B_{\max}$ with the largest known number of flux vacua [4], and universally in large ensembles that have been studied recently [5, 35, 36]. $4d$ NHC give rise to interesting features [37] (such as loops and branches) not present in $6d$. $6d$ NHC have also been studied extensively [30, 38–43], in the context of both $6d$ string universality and $(1,0)$ SCFTs.

Non-Higgsable clusters can be studied for general bases B, see e.g. [37], but since our examples will be in the case that B is a toric variety, we will specialize to that case immediately. A compact toric variety B is specified by a complete fan that is made up of rays v_i that generate cones whose union determines the fan. For most of what we do in this paper, the v_i will play a starring role and the cone structure will be less important. For example, for $\dim_{\mathbb{C}}(B) = 3$ as in our case, the monomials that may appear in f and g are determined by integral points of the polyhedra

$$\Delta_f = \{m \in \mathbb{Z}^3 \,|\, m \cdot v_i + 4 \geq 0 \;\forall i\} \qquad \Delta_g = \{m \in \mathbb{Z}^3 \,|\, m \cdot v_i + 6 \geq 0 \;\forall i\} \tag{4.4}$$

by the correspondence

$$m_f \in \Delta_f \;\mapsto\; \prod_i x_i^{m_f \cdot v_i + 4} \qquad m_g \in \Delta_g \;\mapsto\; \prod_i x_i^{m_g \cdot v_i + 6}, \tag{4.5}$$

which may appear in f and g, respectively, and where each x_i is a homogeneous coordinate on B that is in one to one correspondence with v_i. The most general f and g are therefore of the form

$$f = \sum_{m_f \in \Delta_f} a_f \prod_i x_i^{m_f \cdot v_i + 4} \qquad g = \sum_{m_g \in \Delta_g} a_g \prod_i x_i^{m_g \cdot v_i + 6}, \tag{4.6}$$

where no restrictions are made on the monomial coefficients. By studying Δ_f and Δ_g, it is a straightforward combinatoric exercise to determine the components (overall factors) of f and g, and therefore the non-Higgsable clusters. The mentioned example of $\mathbb{F}_3$ with a non-Higgsable SU(3), for example, has $\{v_i\} = \{(1,0),(0,1),(-1,0),(-1,-3)\}$. By computing Δ_f and Δ_g to construct the most general f and g, one will find a factorization that give the NH7.

4.2 A large ensemble of F-theory geometries

Since it is central to our machine learning analysis, let us review the construction of [5] that gives rise to $\frac{4}{3} \times 2.96 \times 10^{755}$ F-theory geometries.

The construction performs a large number of topological transitions away from an initial algebraic threefold B_i, generating a large number of other threefolds, and then uses them as F-theory bases B. The Calabi-Yau elliptic fibrations over these B form one connected moduli space with many branches, and all of the B are different algebraic varieties.

Specifically, the initial threefold B_i is a smooth weak-Fano toric threefold, which can be specified by a fine regular star triangulation (FRST) of a three-dimensional reflexive polytope Δ°; using machine learning to estimate the number of such triangulations was the subject of section 3. The fan associated to B_i is composed of 2-cones and 3-cones that appear as edges and faces (triangles) on the real codimension one faces of Δ° in $\mathbb{Z}^3$, which are known as facets. The number of edges and faces in the facet are determined by the number of boundary and interior points in the facet, and these numbers are triangulation independent. The largest facets which appear in the ensemble of 4319 reflexive polytopes are

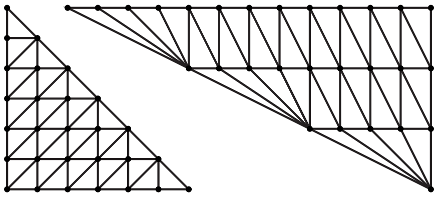

and this is the sort of picture the reader should have in mind when we refer to building structure on the "ground"; this is the ground.

The topological transitions are smooth blow-ups along curves or points. In the former case, two 3-cones labeled by their generators (v_1, v_2, v_3) an (v_4, v_2, v_3) are replaced by (v_1, v_2, v_e), (v_1, v_3, v_e), (v_4, v_2, v_e), (v_4, v_3, v_e), where $v_e = v_2 + v_3$ lies above the original facet in which v_1, v_2, v_3, v_4 lie. The process can be iterated multiple times, for example doing a similar subdivision that adds new rays $v_f = v_e + v_2 = v_1 + 2v_2$ and $v_g = v_e + v_1 = 2v_1 + v_2$. The new structure could be visualized in three dimensions as

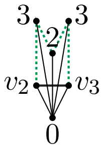

where the solid line in between v_2 and v_3 is the edge on the facet, or ground, above which the new rays have been added; we may refer to edges or faces above which new rays are added as *patches* on the ground. This structure is the result of a sequence of blowups, and rather than continually saying "sequence of blowups" we will instead refer to the rays and cone structure associated to the sequence of blow-ups as *trees*, as suggested naturally by the image, where the dashed green lines denote new edges above the original patch on the ground. Any new ray v in the fan associated to B may be written as a linear combination $v = av_1 + bv_2 + cv_3$ if it is above a face with vertices v_1, v_2, v_3 or as $v = av_1 + bv_2$ if it is above an edge with vertices v_1, v_2. As the sequence of blow-ups are trees, we will refer to the new rays v in the tree as its *leaves*, each of which has a *height* $h = a + b + c$ or $h = a + b$ depending on whether it is above a face or an edge. The numbers in the picture are the heights of the leaves, and the height measures the distance of the ground. We will interchangeably refer to $h = 1$ leaves as roots, or leaves on the ground, as with these definitions the $h = 1$ leaves were already in the original reflexive polytope Δ°. The height of a tree is defined to be the height of its highest leaf.

Trees built above faces will be referred to as *face trees*, and those above edges will be referred to as *edge trees*. It is possible to classify the number of face trees and edge trees with a fixed maximal height $h \leq N$. It is convenient to view the edges and trees face on, i.e. with the leaves projected onto the edge from above. In this case the edge on the ground appears as

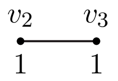

with the edge vertices and their heights labeled. Adding $v_1 + v_2$ subdivides the edge, and further subdividing, dropping vertex labels, gives

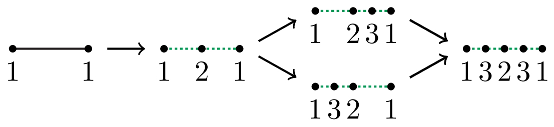

which are all of the $h \leq 3$ edge trees. Similarly, the face trees may be viewed face on, and beginning with a face the first blowup gives

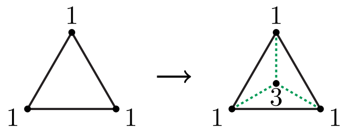

which are the only two $h \leq 3$ face trees. The green dotted lines in both pictures denote edges that are above the original ground, due to at least one of the leaves on the edge having $h > 1$, i.e. being above the ground.

Also critical to the construction is a bound $h \leq 6$ on all trees. This bound is sufficient, but not necessary, to avoid a pathology known as a $(4, 6)$ divisor that is not allowed in a consistent F-theory compactification; see the appendix of [5] for an in-depth discussion. Given this bound, it is pertinent to classify all $h \leq 6$ face trees and edge trees. Their number, for all $3 \leq N \leq 6$, is

N	# Edge Trees	# Face Trees
3	5	2
4	10	17
5	50	4231
6	82	$41,873,645$

and these numbers enter directly into the combinatorics that generate the large ensemble.

The ensemble S_{Δ° associated to a $3d$ reflexive polytope is defined as follows. First, pick a fine regular star triangulation of Δ°, denoted $\mathcal{T}(\Delta^\circ)$. Add one of the $41,873,645$ face trees to each face of $\mathcal{T}(\Delta^\circ)$, and one of the 82 edge trees to each edge of $\mathcal{T}(\Delta^\circ)$. The size of S_{Δ° is

$$|S_{\Delta^\circ}| = 82^{\#\tilde{E}\,\text{on}\,\mathcal{T}(\Delta^\circ)} \times (41,873,645)^{\#\tilde{F}\,\text{on}\,\mathcal{T}(\Delta^\circ)}\,, \tag{4.7}$$

where $\#\tilde{E}$ and $\#\tilde{F}$ are the number of edges and faces on $\mathcal{T}(\Delta^\circ)$, which are triangulation-independent and are entirely determined by Δ° [44].

Two of the $3d$ reflexive polytopes give a far larger number $|S_{\Delta^\circ}|$ than all of the others combined. These polytopes are the convex hulls $\Delta_i^\circ := \text{Conv}(S_i), i = 1, 2$ of the vertex sets

$$\begin{aligned} S_1 &= \{(-1,-1,-1), (-1,-1,5), (-1,5,-1), (1,-1,-1)\}\,, \\ S_2 &= \{(-1,-1,-1), (-1,-1,11), (-1,2,-1), (1,-1,-1)\}. \end{aligned}$$

Surprisingly, $\mathcal{T}(\Delta_1^\circ)$ and $\mathcal{T}(\Delta_2^\circ)$ have the same number of edges and faces. Their largest facets were the ones previously displayed, and they have $\#\tilde{E} = 63$ and $\#\tilde{F} = 36$. This gives

$$|S_{\Delta_1^\circ}| = \frac{2.96}{3} \times 10^{755} \qquad |S_{\Delta_2^\circ}| = 2.96 \times 10^{755}, \tag{4.8}$$

where the factor of 1/3 is due to a particular $\mathbb{Z}_3$ rotation that gives an equivalence of toric varieties; see the appendix of [5] for a discussion. All of the other polytopes Δ° contribute negligibly, yielding $|S_{\Delta^\circ}| \leq 3.28 \times 10^{692}$ configurations. This gives

$$\#\text{ 4d F-theory Geometries} \geq \frac{4}{3} \times 2.96 \times 10^{755}, \tag{4.9}$$

which is a lower bound for a number of reasons discussed in [5].

We end this section with a critical technical point. Previously we described how to read off the non-Higgsable gauge group for fixed base B by constructing the Δ_f and Δ_g polytopes (4.4), their associated monomials (4.5), and from them the most general possible f and g.

We have just introduced a large number of topological transitions $B \to B'$, and via these transitions the gauge groups on various leaves may change. The minimal transitions $B \to B'$ arise as from a single blow-up, which adds an exceptional divisor $x_e = 0$ and new ray $v_e = 0$ that wasn't present in the set of rays associated to B. Adding this new ray means that in (4.4) there is an additional upper half plane condition that must be satisfied. If these upper half planes slice across Δ_f and Δ_g, they are changed

$$\Delta_f \mapsto \Delta_f' \qquad \Delta_g \mapsto \Delta_g', \tag{4.10}$$

where Δ_f' (Δ_g') contains all points of Δ_f (Δ_g) except those removed by the new upper half plane $m \cdot v_e + 4 \geq 0$ ($m \cdot v_e + 6 \geq 0$). In such a case we say that the points $m_f \in \Delta_f$ ($m_g \in \Delta_g$) that are removed by the process are "chopped off", since the upper half plane condition forms the new polytope by slicing across the old one and removing those points.

More generally the process $B \to B'$ may be a sequence of transitions, where the full sequence adds a tree. In that case there will be as many new upper half planes as there are new leaves in the tree, and each may chop points out of the original Δ_f (Δ_g) to form Δ_f' (Δ_g').

The critical physical point is that, in doing transitions $B \to B'$ that chop out monomials from Δ_f and Δ_g to arrive at Δ_f' and Δ_g', one must redo the gauge group analysis, and the chopping procedure may change the gauge group on vertices present in both B and B'. This is absolutely central to the physics of the construction, as e.g. for the initial B_i the $v \in \Delta^\circ$ have no gauge group, but they quickly obtain gauge groups once trees are added.

4.3 Data generation from random samples

In this section and section 5 we will utilize random samples to generate data that is studied via machine learning. The random samples are generated as follows.

All samples in this paper focus on the ensemble $S_{\Delta_1^\circ}$, where the $B \in S_{\Delta_1^\circ}$ are forests of trees that are built on the $3d$ reflexive polytope $S_{\Delta_1^\circ}$. In future work, it would be interesting to study similar issues in the other large ensemble, $S_{\Delta_2^\circ}$.

Furthermore, all samples in this paper are built on top of a particular triangulation $\mathcal{T}_p$ of Δ_1°, the so-called pushing triangulation, which exists for any reflexive polytope. For a definition of the pushing triangulation, see [44]. For our purposes it suffices to simply list the three-dimensional cones of $\mathcal{T}_p$, which are presented in table 4.

A single random sample is defined as follows. Given $\mathcal{T}_p$, we add a face tree at random at each face of $\mathcal{T}_p$, using an appropriately rescaled version of the SageMath function `random()`. We then also add an edge tree to each edge at random. In doing so, many leaves are added to the original rays of Δ_1°, and the complete set of all rays together with the associated cone structure define an F-theory base B.

This process may be iterated to generate many random samples, and we studied over $10,000,000$ random samples in this paper.

4.4 Gauge group rank

In this section we study whether machine learning can accurately predict the rank of the geometric gauge group in the large ensemble of F-theory geometries. We will see that it naturally leads to a sharp conjecture for the gauge group rank. While a version of the conjecture was already proven in [5], exemplifying the process leading to the conjecture will be important for guiding the genesis of a new conjecture and theorem in section 5.

Let H_i be the number of height i leaves in B. We seek to train a model A to predict the rank of the resulting gauge group rk(G) on the base B

$$B \longrightarrow (H_1, H_2, H_3, H_4, H_5, H_6) \xrightarrow{A} \mathrm{rk}(G)\,. \tag{4.11}$$

We perform a 10-fold cross validation with sample size 1000 and algorithms LR, LIR, LDA, KNN, CART, NB, SVM. The linear regression gave the best results, having a MAPE of 0.013. The decision function is

$$\begin{aligned}\mathrm{rk}(G) = 302.54 - 1.1102\times 10^{-16}\, H_1 + 3.9996\, H_2 + 1.9989\, H_3 \\ + 1.0007\, H_4 + 1.3601\times 10^{-3}\, H_5 + 1.1761\times 10^{-3}\, H_6.\end{aligned} \tag{4.12}$$

Since height 1 leaves are facet interior points that are always present, $H_1 = 38$ for all samples. This is an important observation, since the lack of variance in H_1 means that the coefficient of H_1 can be included in the definition of the intercept by the linear regression. Noting $304 = 38\times 8$, one can rewrite the above equation equivalently as

$$\begin{aligned}\mathrm{rk}(G) = -1.46 + 8\, H_1 + 3.9996\, H_2 + 1.9989\, H_3 \\ + 1.0007\, H_4 + 1.3601\times 10^{-3}\, H_5 + 1.1761\times 10^{-3}\, H_6.\end{aligned} \tag{4.13}$$

This is the output of the linear regression.

We wish to turn the output of machine learning into a sharp conjecture given the rest of the information that we know about the problem. Our choice to redefine the intercept and the effectively constant H_1 term already reflected some underlying knowledge of the F-theory context, as we shall soon see. To go further, note that any leaf can only contribute an integer to the rank of the gauge group; we therefore round all coefficients to the nearest

v_1	v_2	v_3	v_1	v_2	v_3
$(-1,-1,-1)$	$(-1,-1,0)$	$(-1,0,-1)$	$(-1,-1,-1)$	$(-1,-1,0)$	$(-1,0,-1)$
$(-1,-1,-1)$	$(-1,-1,0)$	$(0,-1,-1)$	$(-1,-1,-1)$	$(-1,0,-1)$	$(0,-1,-1)$
$(-1,-1,-1)$	$(-1,0,-1)$	$(0,-1,-1)$	$(-1,-1,5)$	$(-1,-1,4)$	$(0,-1,2)$
$(-1,-1,5)$	$(-1,-1,4)$	$(-1,0,4)$	$(-1,5,-1)$	$(-1,-1,0)$	$(-1,0,0)$
$(-1,-1,5)$	$(-1,-1,4)$	$(0,-1,2)$	$(-1,5,-1)$	$(-1,4,-1)$	$(0,2,-1)$
$(-1,-1,5)$	$(-1,0,4)$	$(0,-1,2)$	$(-1,5,-1)$	$(-1,-1,4)$	$(-1,4,0)$
$(-1,5,-1)$	$(-1,-1,0)$	$(-1,0,0)$	$(-1,5,-1)$	$(-1,0,0)$	$(-1,1,0)$
$(-1,5,-1)$	$(-1,-1,0)$	$(-1,4,-1)$	$(-1,5,-1)$	$(-1,0,1)$	$(-1,3,0)$
$(-1,5,-1)$	$(-1,4,-1)$	$(0,2,-1)$	$(-1,5,-1)$	$(-1,0,2)$	$(-1,3,0)$
$(-1,5,-1)$	$(-1,-1,4)$	$(-1,0,3)$	$(-1,5,-1)$	$(-1,1,0)$	$(-1,2,0)$
$(-1,5,-1)$	$(-1,-1,4)$	$(-1,4,0)$	$(1,-1,-1)$	$(-1,-1,0)$	$(0,-1,-1)$
$(-1,5,-1)$	$(-1,4,0)$	$(0,2,-1)$	$(1,-1,-1)$	$(-1,0,-1)$	$(0,0,-1)$
$(-1,5,-1)$	$(-1,0,0)$	$(-1,1,0)$	$(1,-1,-1)$	$(-1,2,-1)$	$(0,0,-1)$
$(-1,5,-1)$	$(-1,0,1)$	$(-1,2,0)$	$(1,-1,-1)$	$(-1,4,-1)$	$(0,1,-1)$
$(-1,5,-1)$	$(-1,0,1)$	$(-1,3,0)$	$(-1,-1,2)$	$(-1,0,1)$	$(-1,1,1)$
$(-1,5,-1)$	$(-1,0,2)$	$(-1,2,1)$	$(-1,-1,2)$	$(-1,0,2)$	$(-1,1,1)$
$(-1,5,-1)$	$(-1,0,2)$	$(-1,3,0)$	$(1,-1,-1)$	$(-1,-1,4)$	$(0,-1,1)$
$(-1,5,-1)$	$(-1,0,3)$	$(-1,1,2)$	$(1,-1,-1)$	$(-1,0,4)$	$(0,-1,2)$
$(-1,5,-1)$	$(-1,1,0)$	$(-1,2,0)$	$(1,-1,-1)$	$(-1,2,2)$	$(0,0,1)$
$(-1,5,-1)$	$(-1,1,2)$	$(-1,2,1)$	$(1,-1,-1)$	$(-1,4,0)$	$(0,1,0)$
$(1,-1,-1)$	$(-1,-1,0)$	$(0,-1,-1)$	$(-1,0,1)$	$(-1,1,1)$	$(-1,3,0)$
$(1,-1,-1)$	$(-1,0,-1)$	$(0,-1,-1)$	$(-1,-1,0)$	$(-1,-1,1)$	$(-1,0,0)$
$(1,-1,-1)$	$(-1,0,-1)$	$(0,0,-1)$	$(-1,-1,0)$	$(-1,0,-1)$	$(-1,1,-1)$
$(1,-1,-1)$	$(-1,-1,0)$	$(0,-1,0)$	$(-1,-1,0)$	$(-1,1,-1)$	$(-1,2,-1)$
$(1,-1,-1)$	$(-1,2,-1)$	$(0,0,-1)$	$(-1,-1,0)$	$(-1,2,-1)$	$(-1,3,-1)$
$(1,-1,-1)$	$(-1,2,-1)$	$(0,1,-1)$	$(-1,-1,0)$	$(-1,3,-1)$	$(-1,4,-1)$
$(1,-1,-1)$	$(-1,4,-1)$	$(0,1,-1)$	$(-1,-1,1)$	$(-1,-1,2)$	$(-1,0,1)$
$(1,-1,-1)$	$(-1,4,-1)$	$(0,2,-1)$	$(-1,-1,1)$	$(-1,0,0)$	$(-1,1,0)$
$(-1,-1,2)$	$(-1,0,1)$	$(-1,1,1)$	$(-1,-1,1)$	$(-1,1,0)$	$(-1,2,0)$
$(1,-1,-1)$	$(-1,-1,2)$	$(0,-1,0)$	$(-1,-1,2)$	$(-1,-1,3)$	$(0,-1,1)$
$(-1,-1,2)$	$(-1,0,2)$	$(-1,1,1)$	$(-1,-1,3)$	$(-1,-1,4)$	$(0,-1,1)$
$(1,-1,-1)$	$(-1,-1,2)$	$(0,-1,1)$	$(-1,-1,3)$	$(-1,0,3)$	$(-1,1,2)$
$(1,-1,-1)$	$(-1,-1,4)$	$(0,-1,1)$	$(-1,-1,4)$	$(-1,0,4)$	$(-1,1,3)$
$(1,-1,-1)$	$(-1,-1,4)$	$(0,-1,2)$	$(-1,-1,4)$	$(-1,1,3)$	$(-1,2,2)$
$(1,-1,-1)$	$(-1,0,4)$	$(0,-1,2)$	$(-1,-1,4)$	$(-1,2,2)$	$(-1,3,1)$
$(1,-1,-1)$	$(-1,0,4)$	$(0,0,1)$	$(-1,-1,4)$	$(-1,3,1)$	$(-1,4,0)$

Table 4. The three-dimensional cones of the pushing triangulation $\mathcal{T}_p$ of Δ_1°.

integer. Second, all divisors in B in our language are given by a leaf with some height. Since seven-branes are wrapped on divisors, it is natural to expect that with appropriate variables that capture important properties of divisors, such as H_i, the intercept should be close to zero; it is -1.46, which is quite close given that typical values of $\text{rk}(G)$ are $O(2000)$. With these considerations taken into account,

$$\text{rk}(G) \simeq 8\, H_1 + 4\, H_2 + 2\, H_3 + \, H_4. \tag{4.14}$$

Recalling that each leaf can only have a geometric gauge group contained in the set

$$G \in \{E_8, E_7, E_6, F_4, D_4, B_3, G_2, A_2, A_1\}, \tag{4.15}$$

it is natural to make the following conjecture based on this analysis:

Conjecture. *With high probability, height* 1 *leaves have gauge group* E_8*, height* 2 *leaves have gauge group* F_4*, height* 3 *leaves have gauge group* G_2 *or* A_2*, and height* 2 *leaves have gauge group* A_1*.*

This conjecture is the natural output of the discussed machine learning analysis, linear regression fit, and basic knowledge of the dataset. The natural questions to ask are what constitutes high probability, are there important counterexamples that lead to sub-cases of the conjecture, and how does one go about proving it.

There is one item of critical importance: this conjecture arose out of a set of random samples, and therefore proving the conjecture may depend on particular properties P_i of the random samples. In this context, "with high probability" could mean that the conjecture depends critically on properties with high probability $P(P_i)$. A natural proof method, then, is to identify those high probability properties, and try to use them to prove the conjecture.

By studying random samples, it quickly becomes clear that nearly all $h = 1$ leaves carry E_8, and in particular in all random samples computed to date there are ≥ 36 out of a possible 38 $h = 1$ leaves that carry an E_8. This means that nearly all leaves are built "above" E_8 roots, meaning that the associated v are linear combinations of v_i's that carry E_8. Since E_8 on $h = 1$ leaves is so probable, this leads to

Refined Conjecture. *Let* v *be a leaf* $v = av_1 + bv_2 + cv_3$ *built on roots* $v_{1,2,3}$ *whose associated divisors carry* E_8*. Then if the leaf has height* $h_v = 2, 3, 4$ *its associated gauge groups are* F_4*,* $\in \{G_2, A_2\}$*, and* A_1*, respectively.*

With this level of refinement, it is possible to do precise calculations leading to the proof of the conjecture, and a final refinement of the gauge group for height 3 leaves. In fact, a version of this conjecture has already been proven in [5]. The precise result is

Theorem. *Let* v *be a leaf* $v = av_1 + bv_2 + cv_3$ *with* v_i *simplex vertices in* F*. If the associated divisors* $D_{1,2,3}$ *carry a non-Higgsable* E_8 *seven-brane, and if* v *has height* $h_v = 1, 2, 3, 4, 5, 6$ *it also has Kodaira fiber* $F_v = II^*, IV^*_{ns}, I^*_{0,ns}, IV_{ns}, II, -$ *and gauge group* $G_v = E_8, F_4, G_2, \text{SU}(2), -, -$*, respectively.*

The proof is short and is presented in the appendix of [5].

At this point the reader is probably wondering why we went through a non-trivial exercise to lead to the formulation of a conjecture, when a version of that conjecture has already been proven. It is because in this simple result we see a back and forth process using machine learning and knowledge of the data that led to the formulation of the conjecture, and we believe this process is likely to be of broader use. That process is:

1. *Variable Selection.* Based on knowledge of the data, choose input variables X_i that are likely to determine some desired output variable Y. In the example, this was recognizing that $X_i = H_i$ may correlate strongly with gauge group.

2. *Machine Learning.* Via machine learning, train a model to predict Y given X_i with high probability. In this example, a 10-fold cross validation was performed, and it was noted that the highest accuracy came from a linear regression.

3. *Conjecture Formulation.* Based on how the decision function uses X_i to determine Y, formulate a first version of the conjecture. In this example, the first version of the conjecture arose naturally from the linear regression and basic dataset knowledge.

4. *Conjecture Refinement.* The original conjecture arose from a model that was trained on a dataset that is subject to sampling assumptions. Those assumptions may lead to high probability properties critical to proving the conjecture; refine accordingly based on them. In the example, we used the high frequency of E_8 on the ground.

5. *Proof.* After iterating enough times that the conjecture is precise and natural calculations or proof steps are obvious, attempt to prove the conjecture.

We will use this procedure to produce new results in section 5.

5 Conjecture generation: E_6 sectors in F-theory ensembles

Recently, an ensemble of $\frac{4}{3} \times 2.96 \times 10^{755}$ F-theory geometries was presented and universality properties regarding the gauge group were derived. There, it was shown that certain geometric assumptions lead to the existence of a gauge group G of rank $\text{rk}(G) \geq 160$ with certain detailed properties that correlated with the heights of certain “leaves” that corresponded to divisors in an algebraic threefold. The simple factors in the generically semi-simple group G were $G_i \in \{E_8, F_4, G_2, A_1\}$, which interestingly only have self-conjugate representations. However, E_6 and SU(3) may also exist in this ensemble. In certain random samples they exist with probability $\simeq 1/1000$, but the conditions under which E_6 or SU(3) existed were not identified at that time. In this section we wish to use supervised learning to study the conditions under which E_6 exists in the ensemble. We will name subsections in this section according to the general process outlined in section 4.

5.1 Variable selection

The results of [5] demonstrate that the gauge group on low lying leaves depends on the heights of trees placed at various positions around the polytope. Yet for the E_6 problem that we study, training a model on tree heights did not give as accurate results as we had expected, and led us to consider other natural variables on which to train the model. This is the process of variable selection.

The problem at hand, and for which we are developing new variables, is the problem of determining whether a particular leaf has a particular gauge group on it. This question has a yes or no answer, and therefore this is a classification problem. We will focus on leaves on the ground, but with some modifications the basic idea extends to other leaves as well.

Let v_1 be a leaf on the ground. Since $\text{mult}_v(f) < 4$ or $\text{mult}_v(g) < 6$ for consistency of the compactification, the monomials in f and g with minimal multiplicity along v in f and g satisfy these multiplicity bounds. These must necessarily come from associated points $m_f \in \Delta_f$ and $m_g \in \Delta_g$ satisfying $-4 \leq m_f \cdot v_1 < 0$ or $-6 \leq m_g \cdot v_1 < 0$. Therefore, monomials m with $m \cdot v < 0$ play a central role in determining the gauge group. On the other hand, the above bounds on m_f and m_g are necessary for playing a role in determining the gauge group on v_1, but they are not sufficient, since if $m_f \cdot v < -4$ ($m_g \cdot v < -6$) for some other v then $m_f \notin \Delta_f$ ($m_g \notin \Delta_g$), and then it does not play any role in determining the gauge group. This follows from the definition (4.4) of Δ_f and Δ_g, since all rays v associated to B appear, not just v_1, i.e. the upper half planes associated with all v may in principle chop out m_f and m_g, not just the upper half plane associated to v_1.

The task is to determine those v that could cause m_f or m_g to be chopped off of the original Δ_f or Δ_g, since the gauge group depends on whether or not this occurs to the set of monomials with minimal order of vanishing in f or g. The other fact we have at our disposal is that at least one of the inequalities $m_f \cdot v_1 < 0$ or $m_g \cdot v_1 < 0$ must be satisfied. Let us use the m_f inequality, knowing that similar comments hold for the m_g inequality. Then, for any v that is a leaf in a tree above v_1, we have $v = av_1 + bv_2 + cv_3$ and therefore v chops off m_f if

$$m_f \cdot v = a\, m_f \cdot v_1 + b\, m_f \cdot v_2 + c\, m_f \cdot v_3 < -4. \tag{5.1}$$

Since $m_f \cdot v_1 < 0$, it is easy to see that the larger a is the more likely it is that the latter two terms do not compensate to satisfy the inequality, in which case m_f is chopped off. There may be many such leaves built on v_1 in this way, and they could occur above different simplices, i.e. with v_1 fixed but with different v_2 and v_3. Since whether or not $m_f \in \Delta_f$ depends strongly on leaves v_i with associated a_i built above v_1, the gauge group may also.

With this motivating discussion, let us define the variables on which we train our models. If $v = av_1 + bv_2 + cv_3$, then we define a,b,c to be the *height above* v_1, v_2, v_3, respectively, which sit on the ground. Let

$$S_{a,v_1} := \{v \in V | v = av_1 + bv_2 + cv_3, \;\; b, c \geq 0\} \tag{5.2}$$

for some fixed value of $a > 0$, where V is the set of rays in the fan associated to the toric variety. Note that, depending on the simplex under consideration, there may be several pairs (v_2, v_3). This set is easily computed for any $B \in S_{\Delta^\circ}$, i.e. for any B in the ensemble of [5]. For some a_{max}, $S_{>a_{\text{max}},v_1}$ is empty, and therefore elements of S_{a_{max},v_1} are the most likely to chop out an m_f or m_g relative to elements of $S_{a<a_{\text{max}},v_1}$. Furthermore, if the

cardinality of $S_{a_{\max},v_1}$ is large, there are more chances to chop off m_f. To any $v \in V$ satisfying $v \in \Delta^\circ$ (this latter assumption is for simplicity), we therefore have a map

$$v \mapsto (a_{\max}, |S_{a_{\max},v}|) \qquad \forall v \in \Delta^\circ, \tag{5.3}$$

and these will be the set of training variables that we will use.

In summary, instead of training on the *heights* of leaves distributed throughout Δ°, we will instead train on the number of leaves of maximal *height above* each $v \in \Delta^\circ$. An analytical argument was presented above for why these might be relevant for the gauge group, but due to the complexity of the sets $S_{a_{\max},v}$ it is not obvious how to concretely extract gauge group information. This is therefore an ideal test case to employ machine learning techniques.

5.2 Machine learning

Let us now turn specifically to the study of E_6 gauge groups that arise in $S_{\Delta_1^\circ}$. In a million random samples, E_6 only arose on a particular distinguished vertex

$$v_{E_6} = (1, -1, -1), \tag{5.4}$$

which is the only vertex of Δ_1° not in its biggest facet. However, E_6 arose on this vertex with probability $\sim 1/1000$, and (due in part to potential phenomenological relevance) it is of interest to understand this result better. Specifically, one would like to have a better understanding of the conditions under which E_6 arises, and whether the probability is a general result or something that is specific to assumptions of the random sampling.

Specifically, we will use these variables to train a model to predict whether or not a given B in a random sample has E_6 on v_{E_6}. This model defines a map A

$$\Delta_1^\circ \longrightarrow (a_{\max}, |S_{a_{\max},v}|)\, \forall v \in \Delta_1^\circ \xrightarrow{A} E_6 \text{ on } v_{E_6} \text{ or not}, \tag{5.5}$$

and the goal is to obtain maximal accuracy. For classification problems, such as this one, accuracy simply means whether A makes the correct prediction amongst a class of possibilities, which in this case is a binary class.

We will train on 20,000 samples, but in this particular case it is important to change the sampling prescription slightly. Under a purely random sample, approximately 20 of the cases sampled would indeed have E_6 on v_{E6} and the rest would not. In this case, the trained algorithm will naturally lead to a constant prediction of no E_6 for all inputs, and it would have accuracy .999. This is clearly a sub-optimal outcome with a misleading accuracy value. To correct for this possibility we will use random sampling to generate 10,000 samples with E_6 and 10,000 without, training on the combined set.

Using this dataset, we perform a 10-fold cross validation using algorithms LR, LDA, KNN, CART, SVM, and a validation size of 0.2, which reduces the training set to have 16,000 samples and the validation set to have 4000. The results are presented in figure 4, and we see that all of the models achieve high accuracy, with maximal median accuracy of .995 achieve by the LR and LDA models.

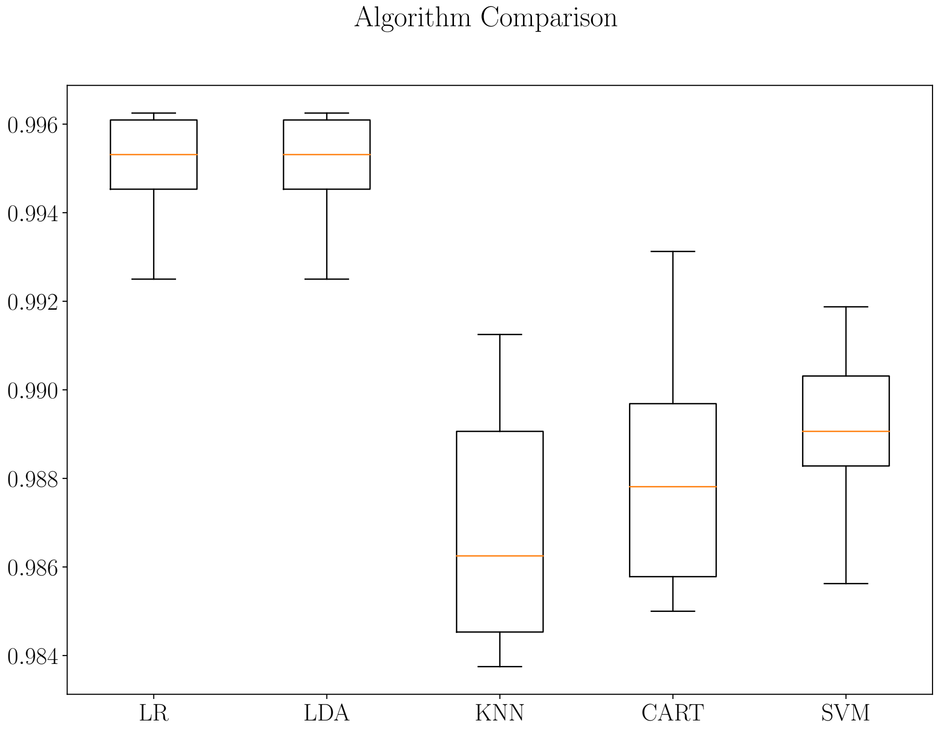

Figure 4. Model comparison from 10-fold cross validation for E_6 sectors. All algorithms perform quite well, though logistic regression and linear discriminant analyses give the best results.

Though we see high accuracy on the enriched samples with 50% E_6 on v_{E_6} and 50% not, it is also interesting to ask whether the models trained on the 50/50 set can make predictions on an unenriched set with E_6 occurring naturally with probability $1 \simeq 1000$. We trained the models on the 50/50 training set, and scored them on the 50/50 validation set of size 4000 and unenriched set of size 20,000, with accuracy:

	LR	LDA	KNN	CART	SVM
50/50 Validation Set	.994	.994	.982	.987	.989
Unenriched Set	.988	.988	.981	.988	.983.

We see that all models accurately predict whether or not there is E_6 on v_{E6} in the unenriched data, even though the models were trained on the 50/50 enriched data. We have done this using $(a_{\max}, |S_{\max,v}|)$ for all v in Δ_1°, which is a set of $2 \times 38 = 76$ integers.

It is natural, however, to ask whether the result is ultimately controlled by some subset of these integers. As discussed in section 2, analyses of this sort are known as *dimensionality reduction*. Applied in this case, a particular type of dimensionality reduction known as a factor analysis demonstrates that, to high accuracy, the question of whether or not E_6 is on v_{E_6} is determined by $(a_{\max}, |S_{a_{\max},v_{E6}}|)$. Specifically, the factor analysis identified that a particular linear combination of the original training variables, which were $(a_{\max}, |S_{a_{\max},v}|)\ \forall v \in \Delta^\circ$, determined whether or not there was an E_6 on v_{E_6}. That linear combination only had non-negligible components along the pair of integers $(a_{\max}, |S_{a_{\max},v_{E6}}|)$. It is natural to expect this, given our previous discussion that motivated the use of these variables in the first place; nevertheless, the factor analysis underscores the relevance of this feature.

Restricting the training data to $(a_{\max}, |S_{a_{\max},v_{E6}}|)$, we performed identical analyses to the previous ones with this restricted set of inputs per example, and find even better accuracy:

	LR	LDA	KNN	CART	SVM
50/50 Validation Set	.994	.994	.994	.994	.994
Unenriched Set	.988	.988	.988	.988	.983.

Thus, we see that there is a single pair of variables, $(a_{\max}, |S_{\max,v_{E6}}|)$, that determines to high accuracy whether or not there is an E_6 factor on v_{E6}! Machine learning has validated the loose ideas as to why $(a_{\max}, |S_{\max,v}|)$ might in some cases be relevant variables from which to predict gauge groups.

5.3 Conjecture formulation

Heartened by the accuracy of the model and the simplicity of the input data, we would like to use it to formulate a conjecture that can be proven rigorously.

To formulate a conjecture using the machine learned model there are two natural paths. One is to look under the hood of the algorithm used to fit the model, study the decision function, and see how it makes predictions given certain inputs. This was the path taken in section 4. For datasets with low dimensionality (or low effective dimensionality after dimensionality reduction) it may be possible to directly examine the predictions for each input and see if there is any obvious trend. For the dimensionally reduced input data that we just discussed, there are in fact only 32 unique pairs $(a_{\max}, |S_{a_{\max},v_{E6}}|)$ in the $20,000$ samples, suggesting that human input may be feasible at this step in the conjecture-generating process.

Utilizing a logistic regression to train a model on these $20,000$ samples, the model makes predictions for whether or not there is an E_6 on v_{E_6} as a function of $(a_{\max}, |S_{a_{\max},v_{E6}}|)$, with the predictions given in table 5. There is an obvious trend: it always predicts no for $a_{\max} = 5$, and usually predicts yes for $a_{\max} = 4$. This is highly suggestive that whether $a_{\max}$ is 4 or 5 for v_{E6} correlates strongly with whether or not there is an E_6. The hyperplane distance is an intrinsic measure of the confidence of the prediction based on the logistic regression. The conclusions of this analysis lead to

Conjecture. *If $a_{\max} = 5$ for v_{E6}, then v_{E6} does not carry E_6. If $a_{\max} = 4$ for v_{E6} it may or may not carry E_6, though it is more likely that it does.*

The initial conjecture is rough, as was the initial conjecture of section 4.

5.4 Conjecture refinement and proof

We now attempt a conjecture refinement based on the sampling assumptions, the high probability properties to which they lead, and general knowledge of the problem at hand.

As discussed, e.g., in [20], a necessary condition for v_{E6} to carry E_6 is that

$$g = x_{E_6}^4 (m^2 + \dots), \tag{5.6}$$

$a_{\max}$	$\lvert S_{a_{\max},v_{E6}}\rvert$	Pred. for E_6 on v_{E_6}	Hyperplane Distance
4	5	No	0.88
4	6	No	0.29
4	7	Yes	-0.31
4	8	Yes	-0.90
4	9	Yes	-1.50
4	10	Yes	-2.09
4	11	Yes	-2.69
4	12	Yes	-3.28
4	13	Yes	-3.88
4	14	Yes	-4.47
4	15	Yes	-5.07
4	16	Yes	-5.67
4	17	Yes	-6.26
4	18	Yes	-6.85
4	19	Yes	-7.45
4	20	Yes	-8.04
4	21	Yes	-8.64
4	22	Yes	-9.23
4	23	Yes	-9.83
4	24	Yes	-10.42
5	1	No	7.34
5	2	No	6.75
5	3	No	6.15
5	4	No	5.56
5	5	No	4.96
5	6	No	4.37
5	7	No	3.78
5	8	No	3.18
5	9	No	2.59
5	10	No	1.99
5	11	No	1.40
5	12	No	0.80

Table 5. Predictions of our logistic regression model as a function of $(a_{\max}, |S_{\max,v_{E_6}}|)$.

where x_{E_6} is the homogeneous coordinate associated to v_{E_6} and $g_4 = m^2$ is a single monomial if B is toric.[4] This single monomial corresponds to a single $\tilde{m} \in \mathbb{Z}^3$ satisfying

$$\tilde{m} \cdot v_{E_6} + 6 = 4. \tag{5.7}$$

In 40,000 random samples, whenever E_6 arose the example had

$$\tilde{m} = (-2, 0, 0). \tag{5.8}$$

Henceforth, by $\tilde{m}$ we will mean precisely this vector in $\mathbb{Z}^3$. Finally, in random samples we have empirically only seen the gauge group G on v_{E_6} arising as $G \in \{E_6, E_7, E_8\}$, suggesting that E_6 only arises with high probability if $\tilde{m} = (-2, 0, 0)$. With some hard work, this probability could be computed, but we leave this for future work and instead take it as a hypothesis for our refined conjectures.

These valuable pieces of information, together with our model analysis, suggests that $\tilde{m}$ is critical to obtaining E_6, and furthermore that its should correlate strongly with $a_{\max}$ being 4 or 5. This leads to a refined conjecture based on evidence from the samples:

Refined Conjecture. *Suppose that with high probability the group G on v_{E_6} is $G \in \{E_6, E_7, E_8\}$ and that E_6 may only arise with $\tilde{m} = (-2, 0, 0)$. Then there are two cases related to determining G.*

a) If $a_{\max} = 5$, $\tilde{m}$ cannot exist in Δ_g and the group on v_{E6} is above E_6.

b) If $a_{\max} = 4$, $\tilde{m}$ sometimes exists in Δ_g. If it does then there is an E_6 on v_{E_6}, and if it does not there is an E_7 or E_8 on v_{E_6}.

Attempting to prove this quickly leads to additional realizations that give a final conjecture:

Theorem. *Suppose that with high probability the group G on v_{E_6} is $G \in \{E_6, E_7, E_8\}$ and that E_6 may only arise with $\tilde{m} = (-2, 0, 0)$. Given these assumptions, there are three cases that determine whether or not G is E_6.*

a) If $a_{\max} \geq 5$, $\tilde{m}$ cannot exist in Δ_g and the group on v_{E_6} is above E_6.

b) Consider $a_{\max} = 4$. Let $v_i = a_i v_{E_6} + b_i v_2 + c_i v_3$ be a leaf built above v_{E_6}, and $B = \tilde{m} \cdot v_2$ and $C = \tilde{m} \cdot v_3$. Then G is E_6 if and only if $(B, b_i) > 0$ or $(C, c_i) > 0$ $\forall i$. Depending on the case, G may or may not be E_6.

c) If $a_{\max} \leq 3$, $\tilde{m} \in \Delta_g$ and the group is E_6.

[4] The reason for this form is the following. A necessary condition to have E_6 on $x_{E_6} = 0$ is that $f = x_{E_6}^3 f_3 + \ldots$ and $g = x_{E_6}^3 + \ldots$, where the $\ldots$ are higher order terms in x_{E_6}; this ensures a Kodaira IV^* fiber above $x_{E_6} = 0$. Let $X \xrightarrow{\pi} B$ be a crepant resolution of such a Weierstrass model. Then a generic point $p \in \{x_{E_6} = 0\}$ has $\pi^{-1}(p)$ being a fiber that is a tree of curves that precisely reproduces the affine E_6 Dynkin diagram. However, if a loop is taken in $x_{E_6} = 0$ by encircling $g_4 = 0$, there is a $\mathbb{Z}_2$ monodromy that gives a $\mathbb{Z}_2$ action on the Dynkin diagram, which reduces the gauge group to F_4 rather than E_6. The condition that this doesn't happen — i.e. that $G = E_6$ — is that g_4 is a perfect square $g_4 = m^2$. For this perfect square phenomenon to occur on a toric base for generic complex structure, g_4 must be a single monomial that is a perfect square.

Proof. We will proceed by a number of direct computations to determine the relationship between $a_{\max}$ and whether $\tilde{m} \in \Delta_g$. Recall that $\tilde{m} \in \Delta_g \leftrightarrow \tilde{m} \cdot \tilde{v}_i + 6 \geq 0\ \forall \tilde{v}_i$, where the $\tilde{v}_i$ are any leaves. Direct computation shows that $\tilde{m} \cdot \tilde{v}_i \in \{-2, 0, 2\}$ for those $\tilde{v}_i \in \Delta_1^\circ$, and that v_{E_6} is the only $p \in \Delta_1^\circ$ satisfying $\tilde{m} \cdot v_{E_6} = -2$. Therefore, any leaf v that cuts $\tilde{m}$ out of Δ_g, i.e. $\tilde{m} \cdot v + 6 < 0$, necessarily has a component along v_{E_6}. Let $v = a v_{E_6} + b v_2 + c v_3$, with $a, b, c \geq 0$; normally we require strict inequality, but do not here so that v may be a leaf in a face tree or and edge tree. Given the above set $\{-2, 0, 2\}$, this yields $-2a + 6 \leq \tilde{m} \cdot v + 6 \leq -2a + 2(b + c) + 6$. We study cases of this general inequality. If $a_{\max} = 5$ there is at least one leaf with $a = 5$, and our bound $a + b + c \leq 6$ implies $b + c = 1$. Then $\tilde{m} \cdot v + 6 \leq -10 + 2 + 6 < 0$ and therefore $\tilde{m} \notin \Delta_g$. This enhances the gauge group on v_{E_6} beyond E_6, proving a). On the other hand, if $a_{\max} = 3$, $\tilde{m} \cdot v + 6 \geq -6 + 6 = 0$ and $\tilde{m} \in \Delta_g$, proving c). The case that requires some work is b), which has $a_{\max} = 4$. Let B, C be $\tilde{m} \cdot v_2$, $\tilde{m} \cdot v_3$. The most constraining leaves are those v with $a = a_{\max}$, in which case $\tilde{m} \cdot v + 6 = -2 + bB + cC$. From above, we have $B, C \in \{0, 2\}$ and $(b, c) \in \{(1, 0), (0, 1), (1, 1)\}$. Then $\tilde{m} \cdot v + 6 \geq 0 \leftrightarrow b$ and B are non-zero or c and C are non-zero. This must occur for all leaves v, in which case G is E_6, proving b).

This theorem is a stronger, rigorous version of the basic result from the model we trained with machine learning, namely that if $a_{\max} = 5$ then the gauge group G on it is above E_6, whereas it may or may not be E_6 if $a_{\max} = 4$.

It is interesting that this result does not depend on triangulation, instead only that a random sampling on some triangulation give $G \in \{E_6, E_7, E_8\}$ with high probability and that E_6 arise with $\tilde{m} = (-2, 0, 0)$. If these assumptions hold in any particular triangulation, then the likelihood of a), b), or c) occurring can be computed explicitly based on the detailed cone structure. Any three-dimensional cone containing v_{E_6} is determined by a 3×3 matrix $M = (v_{E_6}, v_2, v_3)$ subject to the constraint $|\det(M)| = 1$, and from this data B and C can be determined. Without loss of generality we can choose $B \geq C$, and directly compute $(B, C) \in \{(2, 2), (2, 0), (0, 0)\}$. Note that since a leaf in a face tree with height 4 above E_6 is $v = 4 v_{E_6} + b v_1 + c v_2$ and has $b, c > 0$, such a leaf can cut out $\tilde{m}$ only in the case $(B, C) = (0, 0)$. This result is triangulation independent, and we leave the study of other triangulations to future work.

We would like to study the conditions of the theorem in the triangulation from which we built our random samples. The three-cones in this triangulation that contain v_{E_6} are presented in table 6 and all are of $(B, C) = (2, 0)$ type. Therefore in this triangulation face leaves with $a_{\max} = 4$ cannot cut out $\tilde{m}$. Let us consider edge leaves, $v = a v_{E_6} + b v_2$, which we will refer to as an (a, b) edge leaf. Leaves above edges with $a_{\max} = 4$ have $v = 4 v_{E_6} + b v_2$ may be able to cut out $\tilde{m}$ from Δ_g. From part b) of the theorem, this occurs when $B = \tilde{m} \cdot v_2 = 0$, and the only possibility for b is $b = 1$. There are 18 two dimensional cones containing v_{E_6} in our ensemble, 9 with $B = 2$ and 9 with $B = 0$.

This theorem and ensuing discussion imply that E_6 exists on v_{E_6} in this triangulation if and only if there are no $(5, 1)$ edge leaves and there are no $(4, 1)$ edge leaves on edges with $B = 0$. A pertinent fact is that edge trees with $(5, 1)$ edge leaves always also have $(4, 1)$ edge leaves, and therefore the stated condition occurs if and only if there are no $(5, 1)$

v_{E_6}	v_2	v_3
$(1,-1,-1)$	$(-1,-1,0)$	$(0,-1,-1)$
$(1,-1,-1)$	$(-1,0,-1)$	$(0,-1,-1)$
$(1,-1,-1)$	$(-1,0,-1)$	$(0,0,-1)$
$(1,-1,-1)$	$(-1,-1,0)$	$(0,-1,0)$
$(1,-1,-1)$	$(-1,2,-1)$	$(0,0,-1)$
$(1,-1,-1)$	$(-1,2,-1)$	$(0,1,-1)$
$(1,-1,-1)$	$(-1,4,-1)$	$(0,1,-1)$
$(1,-1,-1)$	$(-1,4,-1)$	$(0,2,-1)$
$(1,-1,-1)$	$(-1,-1,2)$	$(0,-1,0)$
$(1,-1,-1)$	$(-1,-1,2)$	$(0,-1,1)$
$(1,-1,-1)$	$(-1,-1,4)$	$(0,-1,1)$
$(1,-1,-1)$	$(-1,-1,4)$	$(0,-1,2)$
$(1,-1,-1)$	$(-1,0,4)$	$(0,-1,2)$
$(1,-1,-1)$	$(-1,0,4)$	$(0,0,1)$
$(1,-1,-1)$	$(-1,2,2)$	$(0,0,1)$
$(1,-1,-1)$	$(-1,2,2)$	$(0,1,0)$
$(1,-1,-1)$	$(-1,4,0)$	$(0,1,0)$
$(1,-1,-1)$	$(-1,4,0)$	$(0,2,-1)$

Table 6. The three-dimensional cones of the pushing triangulation $\mathcal{T}_p$ of Δ_1° that contain v_{E_6}.

edge leaves on $B=2$ edges and no $(4,1)$ edge leaves on $B=0$ edges. Of the 82 possible edge trees, 36 have $(4,1)$ leaves, and 18 have $(5,1)$ leaves. The probability of E_6 on this triangulation T of Δ_1° should then be

$$P(E_6 \,\text{on}\, v_{E_6} \,\text{in}\, T) = \left(1-\frac{36}{82}\right)^9 \left(1-\frac{18}{82}\right)^9 \simeq .00059128. \tag{5.9}$$

This prediction should be checked against random samples. Performing five independent sets of two million random samples each, the predicted number of models with E_6 using this theorem and associated probability, compared to the results from random samples, is

$$\begin{aligned} \text{From Theorem:} \qquad & .00059128 \times 2 \times 10^6 = 1182.56 \\ \text{From Random Samples:} \qquad & 1183,\ 1181,\ 1194,\ 1125,\ 1195. \end{aligned} \tag{5.10}$$

Some statistical variance is naturally expected when sampling, but the agreement is exceptional. Since the probability is computed from a theorem and is reliable when comparing to a random sample, we compute the number of models with E_6 on v_{E_6} given this triangulation:

$$\text{Number of } E_6 \text{ Models on } T = .00059128 \times \frac{1}{3} \times 2.96 \times 10^{755} = 5.83 \times 10^{751}. \tag{5.11}$$

It would be interesting to study phenomenological aspects of these models and whether the probability of E_6 changes in different triangulations of Δ_1°. We leave this to future work.

6 Conclusions

In this paper we have utilized machine learning to study the string landscape. We have exemplified two concepts that we believe will be of broad use in understanding the landscape: deep data dives and conjecture generation.

In a deep data dive, a model trained by machine learning on a subset of a dataset allows for fast and accurate predictions outside of the training set, allowing for fast exploration of the set. In some cases this exploration would not be possible without the model. The example of section 3 is a deep data dive that studies triangulations of $3d$ reflexive polytopes. There, we used machine learning and 10-fold cross validation to optimize a model, eventually selecting an optimized decision tree for our study. This decision tree accurately predicts the average number of fine regular star triangulations per polytope at a given value of h^{11} of the associated toric variety, $\overline{n_{\text{FRST}}}(h^{11})$. These results were already known, providing a basis for evaluating the machine learning results. We found that the decision tree accurately predicts $\overline{n_{\text{FRST}}}(h^{11})$ for five values of h^{11} beyond the training set, though the behavior is erratic at higher h^{11} likely due to being in the tail of the distribution. However, the extrapolation of reliable machine learned data to higher h^{11} accurately predicts the known order of magnitude $\overline{n_{\text{FRST}}}(h^{11} = 35) \sim 10^{15-16}$. In the future machine learning will be used to study Calabi-Yau threefolds in the Kreuzer-Skarke set.

In conjecture generation, machine learning is used to extract hypotheses regarding data features that can lead to the formulation of a sharp conjecture. We found a common procedure that worked for the examples of section 4 and 5: variable selection, machine learning, conjecture formulation, conjecture refinement, proof. Each of the elements is described in section 4, and the section headings of section 5 are chosen according to this procedure. In section 4 we studied the rank of the geometrically non-Higgsable gauge group in an ensemble of $\frac{4}{3} \times 2.96 \times 10^{755}$ F-theory geometries. We used machine learning and 10-fold cross validation to optimize a model, and found that a simple linear regression performed best. This naturally led to a conjecture that the rank of the gauge group depends critically on the number of leaves of a given height in the geometry, and a version of this conjecture had already been proven. In section 5 we studied the appearance of an E_6 factor on a distinguished vertex v_{E_6} in the same ensemble. We again utilized machine learning and 10-fold cross validation to optimize a model, finding that a logistic regression made the most accurate predictions. This led to the generation of a new conjecture regarding when E_6 occurs on v_{E_6}, which was then proven and compared to $10,000,000$ random samples, with good agreement. Both of these sections demonstrated the utility of machine learning in generating conjectures, and underscore the importance of supervision in supervised machine learning: variable selection and dataset knowledge were central to improving the performance of the machine learned models.

We find machine learning a promising way to address big data problems in the string landscape, and find it particularly encouraging that these numerical techniques may lead to rigorous results via conjecture generation.

Acknowledgments

We thank Ross Altman, Tina Eliassi-Rad, Cody Long, and Ben Sung for useful discussions. J.H. is supported by NSF Grant PHY-1620526. B.D.N. is supported by NSF Grant PHY-1620575.

References

[1] R. Bousso and J. Polchinski, *Quantization of four form fluxes and dynamical neutralization of the cosmological constant*, *JHEP* **06** (2000) 006 [hep-th/0004134] [INSPIRE].

[2] S. Ashok and M.R. Douglas, *Counting flux vacua*, *JHEP* **01** (2004) 060 [hep-th/0307049] [INSPIRE].

[3] F. Denef and M.R. Douglas, *Distributions of flux vacua*, *JHEP* **05** (2004) 072 [hep-th/0404116] [INSPIRE].

[4] W. Taylor and Y.-N. Wang, *The F-theory geometry with most flux vacua*, *JHEP* **12** (2015) 164 [arXiv:1511.03209] [INSPIRE].

[5] J. Halverson, C. Long and B. Sung, *On Algorithmic Universality in F-theory Compactifications*, arXiv:1706.02299 [INSPIRE].

[6] F. Denef and M.R. Douglas, *Computational complexity of the landscape. I.*, *Annals Phys.* **322** (2007) 1096 [hep-th/0602072] [INSPIRE].

[7] M. Cvetič, I. Garcia-Etxebarria and J. Halverson, *On the computation of non-perturbative effective potentials in the string theory landscape: IIB/F-theory perspective*, *Fortsch. Phys.* **59** (2011) 243 [arXiv:1009.5386] [INSPIRE].

[8] F. Denef, M.R. Douglas, B. Greene and C. Zukowski, *Computational complexity of the landscape II — Cosmological considerations*, arXiv:1706.06430 [INSPIRE].

[9] N. Bao, R. Bousso, S. Jordan and B. Lackey, *Fast optimization algorithms and the cosmological constant*, arXiv:1706.08503 [INSPIRE].

[10] Y.-H. He, *Deep-Learning the Landscape*, arXiv:1706.02714 [INSPIRE].

[11] F. Ruehle, *Evolving neural networks with genetic algorithms to study the String Landscape*, *JHEP* **08** (2017) 038 [arXiv:1706.07024] [INSPIRE].

[12] D. Krefl and R.-K. Seong, *Machine Learning of Calabi-Yau Volumes*, arXiv:1706.03346 [INSPIRE].

[13] T. Mitchell, *Machine Learning*, McGraw-Hill (1997).

[14] C. Bishop, *Pattern Recognition and Machine Learning*, Springer Publishing Company (2006).

[15] M. Kreuzer and H. Skarke, *Classification of reflexive polyhedra in three-dimensions*, *Adv. Theor. Math. Phys.* **2** (1998) 847 [hep-th/9805190] [INSPIRE].

[16] J. Halverson and J. Tian, *Cost of seven-brane gauge symmetry in a quadrillion F-theory compactifications*, *Phys. Rev.* **D 95** (2017) 026005 [arXiv:1610.08864] [INSPIRE].

[17] C. Vafa, *Evidence for F-theory*, *Nucl. Phys.* **B 469** (1996) 403 [hep-th/9602022] [INSPIRE].

[18] D.R. Morrison and C. Vafa, *Compactifications of F-theory on Calabi-Yau threefolds. 2.*, *Nucl. Phys.* **B 476** (1996) 437 [hep-th/9603161] [INSPIRE].

[19] N. Nakayama, *On Weierstrass models*, in *Algebraic geometry and commutative algebra. Volume II*, Kinokuniya, Tokyo Japan (1988), pp. 405–431.

[20] L.B. Anderson and W. Taylor, *Geometric constraints in dual F-theory and heterotic string compactifications*, *JHEP* **08** (2014) 025 [arXiv:1405.2074] [INSPIRE].

[21] J. Marsano and S. Schäfer-Nameki, *Yukawas, G-flux and Spectral Covers from Resolved Calabi-Yau's*, *JHEP* **11** (2011) 098 [arXiv:1108.1794] [INSPIRE].

[22] C. Lawrie and S. Schäfer-Nameki, *The Tate Form on Steroids: Resolution and Higher Codimension Fibers*, *JHEP* **04** (2013) 061 [arXiv:1212.2949] [INSPIRE].

[23] H. Hayashi, C. Lawrie, D.R. Morrison and S. Schäfer-Nameki, *Box Graphs and Singular Fibers*, *JHEP* **05** (2014) 048 [arXiv:1402.2653] [INSPIRE].

[24] A.P. Braun and S. Schäfer-Nameki, *Box Graphs and Resolutions I*, *Nucl. Phys.* **B 905** (2016) 447 [arXiv:1407.3520] [INSPIRE].

[25] A.P. Braun and S. Schäfer-Nameki, *Box Graphs and Resolutions II: From Coulomb Phases to Fiber Faces*, *Nucl. Phys.* **B 905** (2016) 480 [arXiv:1511.01801] [INSPIRE].

[26] A. Grassi, J. Halverson and J.L. Shaneson, *Matter From Geometry Without Resolution*, *JHEP* **10** (2013) 205 [arXiv:1306.1832] [INSPIRE].

[27] A. Grassi, J. Halverson and J.L. Shaneson, *Non-Abelian Gauge Symmetry and the Higgs Mechanism in F-theory*, *Commun. Math. Phys.* **336** (2015) 1231 [arXiv:1402.5962] [INSPIRE].

[28] A. Grassi, J. Halverson and J.L. Shaneson, *Geometry and Topology of String Junctions*, arXiv:1410.6817 [INSPIRE].

[29] A. Grassi, J. Halverson, F. Ruehle and J.L. Shaneson, *Dualities of Deformed $\mathcal{N} = 2$ SCFTs from Link Monodromy on D3-brane States*, arXiv:1611.01154 [INSPIRE].

[30] D.R. Morrison and W. Taylor, *Classifying bases for* 6*D F-theory models*, *Central Eur. J. Phys.* **10** (2012) 1072 [arXiv:1201.1943] [INSPIRE].

[31] A. Grassi, J. Halverson, J. Shaneson and W. Taylor, *Non-Higgsable QCD and the Standard Model Spectrum in F-theory*, *JHEP* **01** (2015) 086 [arXiv:1409.8295] [INSPIRE].

[32] A.P. Braun and T. Watari, *The Vertical, the Horizontal and the Rest: anatomy of the middle cohomology of Calabi-Yau fourfolds and F-theory applications*, *JHEP* **01** (2015) 047 [arXiv:1408.6167] [INSPIRE].

[33] T. Watari, *Statistics of F-theory flux vacua for particle physics*, *JHEP* **11** (2015) 065 [arXiv:1506.08433] [INSPIRE].

[34] J. Halverson, *Strong Coupling in F-theory and Geometrically Non-Higgsable Seven-branes*, *Nucl. Phys.* **B 919** (2017) 267 [arXiv:1603.01639] [INSPIRE].

[35] J. Halverson and W. Taylor, $\mathbb{P}^1$*-bundle bases and the prevalence of non-Higgsable structure in* 4*D F-theory models*, *JHEP* **09** (2015) 086 [arXiv:1506.03204] [INSPIRE].

[36] W. Taylor and Y.-N. Wang, *A Monte Carlo exploration of threefold base geometries for* 4*d F-theory vacua*, *JHEP* **01** (2016) 137 [arXiv:1510.04978] [INSPIRE].

[37] D.R. Morrison and W. Taylor, *Non-Higgsable clusters for* 4*D F-theory models*, *JHEP* **05** (2015) 080 [arXiv:1412.6112] [INSPIRE].

[38] D.R. Morrison and W. Taylor, *Toric bases for* 6*D F-theory models*, *Fortsch. Phys.* **60** (2012) 1187 [arXiv:1204.0283] [INSPIRE].

[39] W. Taylor, *On the Hodge structure of elliptically fibered Calabi-Yau threefolds*, *JHEP* **08** (2012) 032 [arXiv:1205.0952] [INSPIRE].

[40] D.R. Morrison and W. Taylor, *Sections, multisections and* U(1) *fields in F-theory*, arXiv:1404.1527 [INSPIRE].

[41] G. Martini and W. Taylor, 6*D F-theory models and elliptically fibered Calabi-Yau threefolds over semi-toric base surfaces*, *JHEP* **06** (2015) 061 [arXiv:1404.6300] [INSPIRE].

[42] S.B. Johnson and W. Taylor, *Calabi-Yau threefolds with large* $h^{2,1}$, *JHEP* **10** (2014) 23 [arXiv:1406.0514] [INSPIRE].

[43] W. Taylor and Y.-N. Wang, *Non-toric bases for elliptic Calabi-Yau threefolds and* 6*D F-theory vacua*, arXiv:1504.07689 [INSPIRE].

[44] J.A. De Loera, J. Rambau and F. Santos, *Triangulations: Structures for Algorithms and Applications*, 1st edition, Springer Publishing Company (2010).